

## 14. PHASE CHEMISTRY, FRACTIONAL CRYSTALLIZATION, AND MAGMA MIXING IN BASALTS FROM THE GULF OF CALIFORNIA, DEEP SEA DRILLING PROJECT LEG 64<sup>1</sup>

Michael R. Perfit, Research School of Earth Sciences, Australian National University, Canberra, 2600, Australia, Andrew D. Saunders, Department of Geology, Bedford College, Regent's Park, London NW1 4NS, United Kingdom, and Daniel J. Fornari, Department of Geological Sciences, State University of New York at Albany, Albany, New York

### ABSTRACT

Major-element, trace-element, and mineralogic data from basalts drilled during Leg 64 indicate that a wide spectrum of N-type MORB have been erupted in the Gulf of California. Leg 64 basalts have chemical and mineralogical characteristics broadly similar to those from the East Pacific Rise and Nazca Plate. They are not nearly so evolved as basaltic lavas recovered from the Galapagos Spreading Center. Trace-element data suggest that several N-type mantle sources or a spatially heterogeneous mantle were partially melted to generate the spectrum of basalts recovered during Leg 64. However, simple, closed-system crystal fractionation does not adequately explain all of the observed chemical and mineralogical features. Mixing of primitive magmas, with observed An-rich plagioclase xenocrysts and fractionating magmatic liquids, is a plausible mechanism which can help to explain the evolution of basaltic magmas in the Gulf of California.

### INTRODUCTION

Basalt was cored in Holes 474A, 475B, 477, 477A, 478, and 481A during Leg 64 of the Deep Sea Drilling Project (DSDP). Hole 474A is off the southern end of Baja California on oceanic crust west of the East Pacific Rise. In this hole, drilling penetrated three dolerite sills before encountering a pillow basalt/sill sequence believed to be Oceanic Layer 2. Basalt cobbles were recovered from Hole 475B (located within a slope basin 21 km southeast of Baja), but these are not considered part of an *in situ* flow. Holes 477 and 481 are on the southern and northern rifts, respectively, of the Guaymas Basin and are part of the actively spreading oceanic crust extending from the East Pacific Rise to the San Andreas Fault. At both sites, Quaternary sediments have been intruded by basalt, dolerite, and gabbro sills. Hole 478 was drilled in young oceanic crust 12 km northwest of the active rift; drilling penetrated a sequence similar to the sills intruding turbidites in Holes 477 and 481.

The range of compositions of the major mineral phases in representative samples from Holes 474A, 475B, 477, and 478 have been determined. Petrographic descriptions of the samples are presented in Table 1. Major-element analyses and selected elemental ratios of these samples are presented in Table 2. Detailed accounts of the whole-rock major- and trace-element data are presented in Saunders et al. and Fornari et al. (both papers this volume, Pt. 2, hereafter cited "this volume"). Where a specific whole-rock composition was not measured, the chemical analysis for the nearest sample in the core and unit is presented in Table 2.

We have used the combined petrologic and chemical data to investigate the intra- and intersite relations

among the variety of basalts recovered during Leg 64. In particular, we have tested the hypothesis that fractional crystallization may have played an important role in generating the range of basalt compositions. In light of the tectonic setting of these holes, it is important to see if there are any petrographic or chemical characteristics that distinguish these basalts from other Pacific mid-ocean ridge basalts (MORB).

### MAJOR-ELEMENT VARIATIONS

Complete listings of the major-element compositions of crystalline and glassy basalts are presented in Saunders et al. (this volume) and Fornari et al. (this volume). Only the composition of samples selected for microprobe analysis and representative samples used in fractionation calculations is presented in Table 2. In general, the samples span the entire compositional range of basalts recovered during Leg 64. The basalts range from slightly nepheline normative (Hole 475B) to slightly quartz normative (Hole 474) tholeiites; the majority are subalkaline tholeiites.

Nearly all of the samples plot in the fields defined by Bence et al. (1979) for MORB from the major ocean basins (Figs. 1 and 2). As a whole, the Leg 64 basalts exhibit quite a large degree of chemical diversity and differentiation. For example, Mg numbers ( $Mg/Mg + Fe^{2+} \times 100$ ) vary from  $\sim 75$  in picritic basalt to  $< 55$  in the most fractionated samples (Fig. 3). In detail, basalts from Hole 474 exhibit the greatest variation in Mg number ( $61.5 \pm 5.0$ ) when compared to basalt suites from the other holes, which have more restricted Mg numbers: e.g., Holes 475B ( $66.9 \pm 2.4$ ), 477 ( $65.5 \pm 3.1$ ), 477A ( $60.3 \pm 1.4$ ), 478 ( $67.1 \pm 2.6$ ), and 481A ( $59.5 \pm 2.6$ ). These averages are relatively high, considering that the average Mg number for 600 MORB basalt glasses is 58.6 (Wilkinson, in press) and  $58.8 \pm 2.9$  for 14 Leg 64 glasses analyzed by Fornari et al. (this volume).

<sup>1</sup> Curray, J. R., Moore, D. G., et al., *Init. Repts. DSDP, 64*; Washington (U.S. Govt. Printing Office).

Table 1. Brief petrographic descriptions of analyzed samples.

Sample (interval in cm)	Description
474A-40-2, 38-40 (38)	Olivine-rich dolerite: No primary phenocrysts, but sample contains as much as 30% pseudomorphs of olivine (0.3-3.0 mm). Groundmass contains plagioclase (0.3-0.8 mm) (30%); anhedral, interstitial clinopyroxene (0.3-0.8 mm) (30%); altered olivine (0.3-0.6 mm) (10%); magnetite (5%); subophitic texture.
474A-42-2, 20-23	Dolerite: equigranular with some altered olivine phenocrysts and moderate alteration; minor phenocrysts of plagioclase and spinel with interstitial clinopyroxene.
474A-45-4, 7-9 (10)	Dolerite: subophitic to hyalophitic, containing laths of plagioclase (0.5-2.0 mm) surrounding altered olivine and fresh clinopyroxene phenocrysts (0.25-1.0 mm) in a matrix of plagioclase, clinopyroxene, and glass with abundant titanomagnetite grains.
474A-46-3, 80-82	Basalt: porphyritic with large plagioclase megacrysts (as long as 1 cm) set in a fine matrix of plagioclase olivine, clinopyroxene, and fine opaques.
474A-49-3, 146-149	Pillow basalt: plagioclase phryic, megacryst-rich, with megacrysts as long as 1.5 cm in some sections; microphenocrysts of plagioclase (10%), olivine (5%), and spinel (occasionally clinopyroxene) in an aphanitic matrix with quench textures.
475B-2-1, 0-9 (14)	Olivine basalt: porphyritic with a quenched, variolitic and intersertal texture; anhedral to subhedral olivine phenocrysts (0.2-2.0 mm) (10%); no plagioclase phenocrysts; skeletal, elongate olivine microlites (~5%) and plagioclase microlites (50%) in the groundmass; some in variolitic clusters; approximately 20% clinopyroxene and 10% iron-titanium oxides lie in about 10% mesostasis.
477-13-2, 145-146 (85)	Plagioclase-phryic dolerite: subophitic to intergranular with plagioclase phenocrysts (as long as 4 mm) (15%) surrounded by smaller plagioclase laths enclosing or partially enclosing anhedral to subhedral grains of clinopyroxene (10%) and olivine (15%); groundmass is composed of plagioclase microlites (~30%), olivine (~10%), clinopyroxene (~10%), magnetite (~5%), and some olivine.
478-42-2, 82-83 (85)	Dolerite: contains large (1-4 mm) clinopyroxene phenocrysts optically enclosing smaller plagioclase (1 mm) laths. Matrix is composed of plagioclase (25%), anhedral, clinopyroxene, olivine and iron-titanium oxides (~20%).
478-51-3, 52-53 (48, 111)	Dolerite with gabbro xenoliths: inequigranular ophitic, with large clinopyroxene (1-6 mm) enclosing plagioclase (0.5-1.5 mm) laths and olivine microphenocrysts; approximately 50% plagioclase, 30% clinopyroxene, 10% olivine, 5% iron-titanium oxides.

Note: The petrographic descriptions are generalized and based on observations made from our own probed sections and thin sections prepared during the cruise. Where petrographic data were used from core intervals other than those of the probed section, the level (in cm) is given in parentheses.

Within each site, the major-element variations occurring with decreasing Mg number define trends on variation diagrams that may be interpreted as a consequence of fractional crystallization. For example, increases in  $Al_2O_3$  with decreasing MgO (Fig. 1) in basalts from Holes 477A, 478, and the more mafic members of 474A may result from the removal of olivine (Ol), clinopyroxene (Cpx), or Ol + Cpx from a magma. Conversely, decreases in  $Al_2O_3$  with decreasing MgO, as observed in Holes 474A and 481A, may be caused by plagioclase-dominated crystal fractionation. Major-element trends in MORB glasses clearly show the effects of plagioclase (Plag) + Ol fractionation (Fig. 1). A continual enrich-

ment of  $TiO_2$  with decreasing Mg number in the Leg 64 basalts is evident (Fig. 2) and is a common feature in most MORB suites. Since Ti is an incompatible element in the major liquidus phases in MORB, the continual enrichment could reflect any combination of Plag, Ol, and Cpx fractionation. Highly evolved FeTi basalts, such as those sampled along the Galapagos Rift (Byerly, 1980; Perfit et al., 1980), are absent from the Leg 64 suites.

The effects of fractional crystallization (or crystal accumulation) are more clearly defined by  $CaO/Al_2O_3$  ratios versus Mg-number variation (Table 2, Fig. 3). In general, there is a gradual increase in the  $CaO/Al_2O_3$

Table 2. Selected major-element compositions of basalts used in fractionation calculations, Leg 64.<sup>a</sup>

Hole	474A											475B						
	42-1	40-1	40-2	39-3	43-1	45-4	46-3	46-2	49-1	49-2	47-1	48-1	50-3	50-4	49-3	4-1	3-1	2-1
Core/Section Level (cm)	6	19	40	148	119	64	74	112	2	31	127	101	91	1	133	2	2	32 <sup>a</sup>
Unit	2	1	1	1	3	6	7	7 <sup>b</sup>	7 <sup>b</sup>	7 <sup>b</sup>	7	7	8	8				
SiO <sub>2</sub>	44.5	44.8	48.1	48.2	49.1	49.2	48.0	49.06	50.27	49.68	49.0	48.3	49.3	48.7	48.4	46.8	47.2	48.06
TiO <sub>2</sub>	1.28	1.54	1.59	1.78	1.97	1.83	1.37	1.70	2.15	2.35	1.40	1.59	2.25	2.27	2.04	1.27	1.33	1.47
Al <sub>2</sub> O <sub>3</sub>	15.2	14.7	14.1	15.6	15.1	16.2	17.0	16.62	16.10	14.94	17.3	16.4	15.2	15.2	16.1	16.2	16.6	18.01
FeO <sup>F</sup>	9.68	10.01	9.22	10.03	9.52	9.74	8.81	10.11	10.46	11.68	8.56	9.55	10.75	10.50	10.45	9.28	9.38	9.22
MnO	0.17	0.16	0.17	0.21	0.17	0.14	0.16	0.20	0.20	0.16	0.16	0.17	0.17	0.16	0.21	0.21	0.14	0.17
MgO	14.87	14.90	11.17	7.07	8.09	6.50	7.60	7.86	6.60	6.85	7.50	7.50	6.70	7.25	6.90	10.68	8.66	8.40
CaO	9.59	9.27	10.21	11.17	11.56	11.53	12.39	11.21	10.25	10.90	12.16	12.31	10.85	10.84	11.70	11.48	11.56	11.36
Na <sub>2</sub> O	2.47	2.37	2.66	3.01	2.62	2.77	2.34	2.63	2.88	2.67	2.44	2.42	2.82	2.80	2.71	2.76	2.90	3.00
K <sub>2</sub> O	0.00	0.03	0.06	0.05	0.07	0.12	0.09	0.23	0.25	0.32	0.08	0.11	0.14	0.23	0.15	0.12	0.17	0.14
P <sub>2</sub> O <sub>5</sub>	0.09	0.13	0.12	0.12	0.19	0.20	0.09	0.11	0.14	0.22	0.12	0.10	0.23	0.26	0.16	0.08	0.09	0.07
LOI	1.22	0.90	1.18	1.20	0.68	0.53	0.00	—	—	—	0.00	0.00	0.21	0.50	0.00	0.00	1.26	—
Total	100.07	99.89	99.63	99.64	100.20	99.79	98.88	99.84	99.38	99.93	99.62	99.45	99.93	99.91	99.95	99.88	100.32	99.99
Mg Number	75.3	74.7	70.6	58.3	62.8	56.9	63.1	60.4	55.3	53.5	63.4	60.9	55.0	57.8	56.7	69.5	64.6	64.1
CaO/Al <sub>2</sub> O <sub>3</sub>	0.631	0.631	0.724	0.716	0.766	0.712	0.729	0.674	0.637	0.730	0.703	0.751	0.714	0.713	0.727	0.709	0.696	0.631

Note: FeO<sup>+</sup> = total Fe calculated as Fe<sup>2+</sup>; Mg number = atomic (Mg/Mg + Fe<sup>2+</sup>) × 100, where FeO/FeO + Fe<sub>2</sub>O<sub>3</sub> = 0.9.

<sup>a</sup> Data from Saunders et al. (this volume).

<sup>b</sup> Natural-glass data from Fornari et al. (this volume).

ratio with diminishing Mg number within the Leg 64 basalts. This suggests that the removal of Ol + Plag dominated the evolutionary trends in residual liquids, as Saunders et al. (this volume) have suggested. In detail, however, decreases in CaO/Al<sub>2</sub>O<sub>3</sub> ratios occur within individual holes (e.g., Holes 477A, 481A). This can only be a result of Cpx-dominated fractionation, since Cpx has much higher CaO/Al<sub>2</sub>O<sub>3</sub> ratios (~4) than any MORB magma. In certain cases, the accumulation of plagioclase (CaO/Al<sub>2</sub>O<sub>3</sub> < 0.54) also lowers the CaO/Al<sub>2</sub>O<sub>3</sub> ratios of the samples. The fractionation is complex, and a single mechanism or assemblage probably cannot relate all of the recovered basalts to each other.

On the basis of trace-element abundances and ratios, Saunders et al. (this volume) have shown that basalts from Leg 64 are chemically similar to N-type MORB, but that at least two different mantle sources may have been involved in generating the chemical differences between samples from the Guaymas Basin and Holes 474 and 475. In fact, there is some evidence suggesting that chemical differences between units in one hole could also reflect chemically distinct parental magmas. Significant differences in major-element abundances of relatively primitive basalts support the concept of multiple sources. For example, relatively unfractionated basalts from Hole 478, with Mg numbers between 69 and 70, have CaO/Al<sub>2</sub>O<sub>3</sub> ratios ranging from ~0.67 to 0.73 and TiO<sub>2</sub> contents from 0.79 to 1.25 wt.%. Assuming basalts with Mg numbers ~70 could be primary melts or derivatives obtained after some olivine fractionation, then the wide variations in chemistry may result from differing degrees of partial melting of a mantle source or melting from chemically distinct source regions.

Before assessing possible differences in melting history and mantle chemistry it is important to place constraints on the role and degree of fractional crystallization and magma mixing in this complex region. The fractionation models are used to test and quantify the hypotheses proposed by Saunders et al. (this volume), which are based on trace-element variations. Trace-element abundance modelling, constrained by the most successful major-element calculations, provides more rigorous tests of the applicability of crystal fractionation

and magma mixing—but this will be presented in detail elsewhere.

## PHASE CHEMISTRY

Mineral analyses were done at the University of Cambridge on an energy dispersive spectrometer (EDS) electron microprobe. Measurement and processing of peaks were done by iterative peak stripping (Statham, 1976) and correction methods are after Sweatman and Long (1969). Typical limits of detection are Na ~0.25%, Mg ~0.16%, Al and Si ~0.10%, and K ~0.05%. Data are tabulated in Tables 3 (plagioclase), 4 (clinopyroxene), 5 (olivine), 6 (iron-titanium oxides) and 7 (spinel).

The samples for microprobe work varied from glassy, phyric basalts to aphyric, coarsely crystalline basalts and dolerites with ophitic textures. As a consequence of relatively rapid cooling, minerals in the glassy basalts show limited degrees of solid solution when compared to minerals in coarser, more crystalline dolerites.

Olivines show the most restricted range of compositional zoning and generally occur as near-liquidus phenocrysts. Olivine relicts occur in many samples, but they have been altered and pseudomorphed by clay minerals, making them unsuitable for analysis. Clinopyroxene occurs as subophitic intergrowths with plagioclase, a common groundmass phase, and rarely as poikilitic crystals or phenocrysts. Plagioclase is a ubiquitous phenocryst and groundmass phase. Plagioclase phenocrysts exhibit optical zonations, and megacrysts are commonly rounded and partially resorbed. Some of these megacrysts appear to be xenocrysts. Microphenocrysts of Cr-Al spinel are rarely present in mafic basalts or enclosed in olivine phenocrysts; they generally contribute >2% of the mode. Titanomagnetite is an abundant groundmass phase and, in some samples coexists with less abundant ilmenite.

### Plagioclase

Plagioclase crystals generally have normal chemical zonations with calcic cores (An<sub>82-70</sub>) and more sodic rims (An<sub>70-50</sub>) (Fig. 4). Groundmass plagioclases tend to be more sodic (as low as An<sub>40</sub>) but can be as calcic (An<sub>70-75</sub>) as larger phenocrysts. Plagioclase megacrysts

Table 2. (Continued).

477				477A				478				481A					
9-1	11-2	12-4	13-2	2-1	2-2	3-1	3-2	42-2	43-2	49-1	51-3	54-1	54-4	15-3	15-3	16-2	17-2
7	61	76	146	7	64	86	17	80	104	63	49	77	2	27	115	111	6
2b	2c	2c	2c	2	2	2	2	4	4	4	4	5	6	1	1	1	1
49.8	48.3	48.1	48.7	47.7	48.5	48.2	49.1	47.7	49.0	47.5	52.0	49.2	49.3	50.1	50.0	49.8	49.4
1.92	1.17	1.48	1.58	1.59	1.76	1.14	1.53	0.79	1.68	0.94	2.13	1.25	1.90	2.25	2.14	1.95	1.98
15.7	17.2	16.2	17.9	17.3	17.4	18.9	18.9	16.4	15.8	17.1	16.6	15.5	13.1	15.4	15.6	15.3	15.2
9.22	8.40	8.97	8.39	8.57	8.69	7.27	7.96	7.87	8.95	7.74	7.13	8.30	9.63	9.79	9.81	9.00	9.35
0.17	0.14	0.16	0.14	0.15	0.15	0.13	0.14	0.14	0.14	0.13	0.13	0.14	0.25	0.17	0.18	0.15	0.15
6.95	9.20	9.75	6.65	8.65	7.23	7.31	6.02	8.80	8.60	8.90	4.13	9.30	9.00	6.82	6.25	7.65	8.05
11.70	11.61	10.87	11.89	12.04	11.81	12.81	12.14	10.34	11.02	11.17	11.20	11.26	11.25	9.90	9.81	10.73	10.56
3.11	2.79	2.76	3.05	2.91	3.10	2.82	2.98	3.02	2.89	2.65	3.29	2.47	2.62	3.22	3.14	2.87	2.68
0.20	0.18	0.23	0.20	0.14	0.25	0.12	0.22	0.31	0.15	0.18	0.89	0.15	0.11	0.51	0.59	0.14	0.16
0.33	0.24	0.25	0.21	0.14	0.23	0.12	0.19	0.18	0.21	0.15	0.52	0.19	0.25	0.34	0.45	0.32	0.29
0.00	0.14	0.33	0.00	0.00	0.00	0.12	0.00	3.74	0.00	2.31	1.54	1.04	1.72	0.00	0.00	0.95	1.00
100.13	100.28	100.10	99.64	100.21	100.08	99.70	100.16	100.17	99.46	99.73	100.28	99.77	100.16	100.04	99.11	99.86	99.85
59.9	68.5	68.3	61.1	66.7	62.2	66.6	60.0	68.9	65.6	69.5	53.5	69.0	65.0	57.9	55.7	62.8	63.1
0.745	0.675	0.671	0.664	0.696	0.679	0.678	0.642	0.630	0.697	0.653	0.675	0.726	0.859	0.643	0.629	0.701	0.695

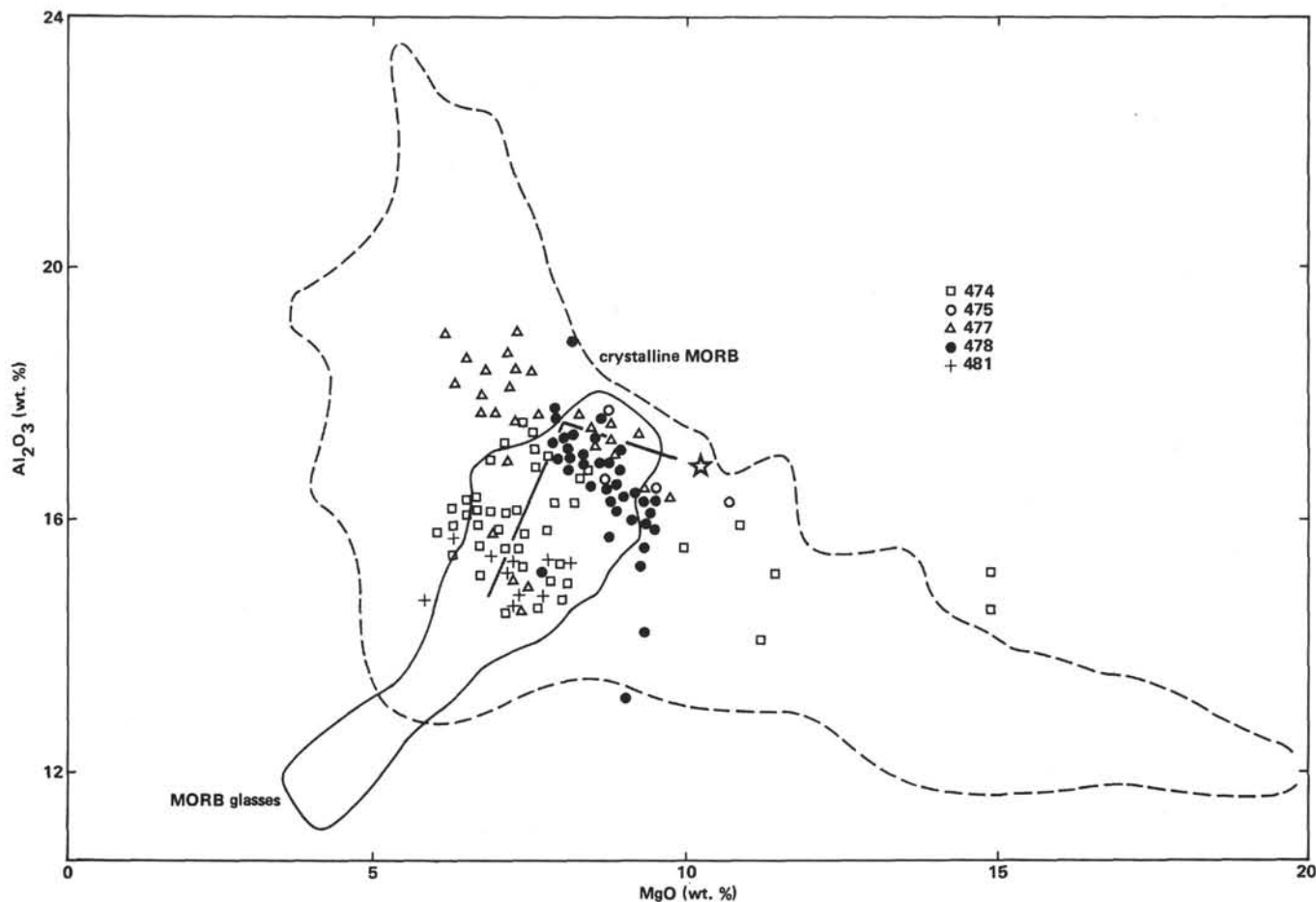


Figure 1. Variation in  $\text{Al}_2\text{O}_3$  versus MgO, Leg 64 basalts. (Data from Saunders et al., this volume; Fornari et al., this volume.) Fields for ~1100 ocean-floor basalt glasses [MORB glasses] and ~1300 crystalline ocean floor basalts [MORB] from Bence et al. [1979] are shown for comparison. Calculated crystal fractionation paths for a FAMOUS basalt composition [Section 572-1-1, indicated by the star] from Bence et al. [1979] for 6% olivine fractionation followed by 24% [Ol + Plag] fractionation in a 1:2 weight proportion are shown.

occur in many basalts recovered during Leg 64. They consistently have more calcic cores ( $\sim \text{An}_{90}$ ) than do co-existing phenocrysts and generally have slightly resorbed rims similar in composition to the phenocryst population ( $\sim \text{An}_{80-64}$ ; Fig. 4, Table 3). The central regions of the megacrysts are only slightly zoned, and the sodic rims are very narrow or absent. Comparison of the  $\text{Ca}/\text{Ca} + \text{Na}$  ratios of the megacryst cores with experimentally determined  $\text{Ca}/\text{Ca} + \text{Na}$  ratios in plagioclase crystallized from natural MORB (see Walker et al., 1979) indicates that the megacrysts are significantly more calcic than would be predicted if they had crystallized in equilibrium with their host magma. The rocks containing megacrysts should have plagioclase phenocrysts with compositions less than  $\sim \text{An}_{80}$ , which, in fact, agrees with the observed phenocryst core compositions (Table 3).

Small amounts of Fe are present in all of the plagioclases analyzed. A positive correlation exists between sodium content and Fe abundance in plagioclase (Fig. 5). The interior portions of megacrysts (highest An) contain the least amount of Fe, whereas their more sodic rims have Fe contents similar to those in phenocryst and groundmass plagioclase. Individual phenocrysts

also show increasing Fe from calcic cores to sodic rims. This trend may be a consequence of increasing Fe + Na content in residual liquids during crystallization of a magma. Mazzullo and Bence (1976) have noted a similar trend in basalts from the Nazca Plate and suggest that the Fe content may not continue to increase during the late stages of crystallization because of the onset of iron-titanium oxide crystallization.

It appears that the megacrysts could not have crystallized from their host basalts and therefore must be considered xenocrysts. The more sodic and slightly resorbed rims are further evidence that these xenocrysts tried to re-equilibrate with the magma. Their presence in many of the basalts suggests the possibility that magma mixing or plagioclase flotation may have occurred during evolution of these basalts.

#### Pyroxene

Pyroxenes in the basalts are predominantly calcic augites (Table 4), and variations in their major end-member components (Wo-En-Fs) are shown in the pyroxene quadrilateral (Fig. 6). Pyroxene crystallization trends involving depletions in Ca with decreasing Mg/Mg + Fe are typical of tholeiitic magmas. Metastable

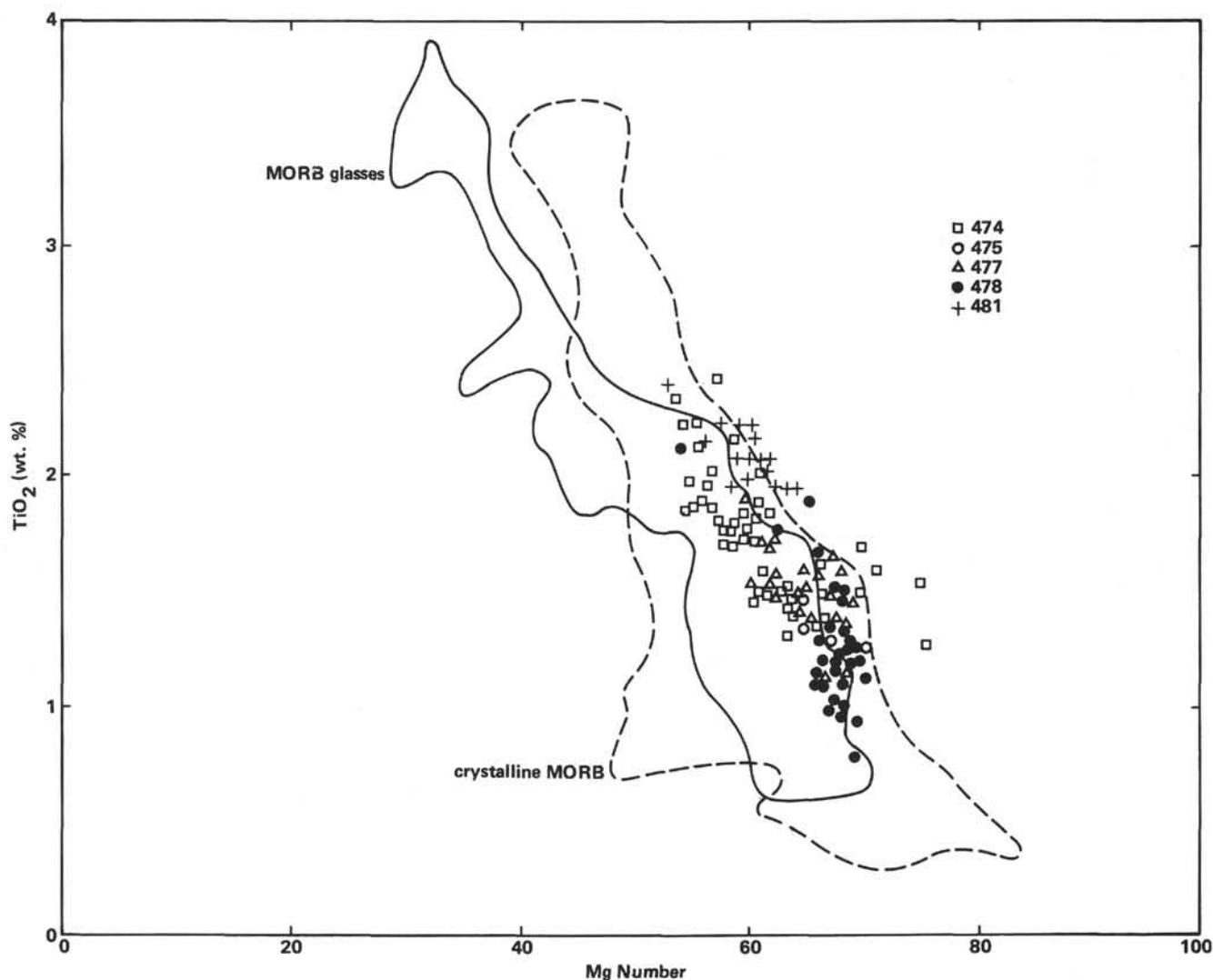


Figure 2.  $\text{TiO}_2$  versus Mg number ( $\text{Mg}/\text{Mg} + \text{Fe}^{2+} \times 100$ ; Fe value used in Mg number calculation = 0.9 FeO) variation diagram, Leg 64 basalts. (Fields for MORB and MORB glasses are shown for comparison [see Fig. 1]. Note somewhat higher  $\text{TiO}_2$  contents at given Mg numbers in Leg 64 basalts.)

low-Ca clinopyroxenes, generally associated with rapid crystallization, do not occur in these basalts.

The percentages of nonquadrilateral components ("others" of Papike et al., 1974) are relatively low (<14%) in all of the pyroxenes. Pyroxenes in basalts from Holes 474A and 477 have greater proportions of "other" components than do pyroxenes from Hole 478 (Table 4). This is primarily a consequence of greater Ti and Al contents in the former. In the classification scheme of Papike et al. (1974) the best pyroxene end-member name for "others" would be CaMg-TAl for Holes 474A and 477; pyroxenes in basalts from Hole 478 would be classified as CaAl-CaTs (Fig. 7). There is a positive correlation between Ti and Al content in all of the pyroxenes at a fairly constant ratio of 1 Ti to 4 Al cations (Fig. 8). This is not a consequence of bulk rock composition, since rocks with the highest and lowest  $\text{TiO}_2$  or  $\text{Al}_2\text{O}_3$  contents contain pyroxenes with similar Ti and Al abundances. Schweitzer et al. (1979) have shown that the Ti-Al<sup>iv</sup> substitution in crystals is one of

the most important "others" pairs in pyroxenes of deep-sea basalts. For comparison with the data presented here, pyroxene data from Leg 34 on the Nazca Plate are plotted in Figure 8 and exhibit the same Ti-Al coupling. Shibata et al. (1979) also make mention of this feature in basalts from the North Atlantic.

Two complementary factors can cause the Ti-Al correlation. Since Ti and Al<sup>iv</sup> vary negatively with Mg (Fig. 9), a Ti-Al buildup during fractionation is possible (Schweitzer et al., 1979). It has been shown, however, that the abundances of Ti and Al will increase with increased cooling rate during experimental pyroxene crystallization (Walker et al., 1976). Textural and mineralogical relations in the Leg 64 basalts suggest that late-stage pyroxenes (i.e., groundmass and poikilitic) contain the greatest amounts of Ti and Al, whereas sub-ophitic-to-euhedral phenocrysts with higher Mg/Mg + Fe<sup>2+</sup> ratios contain less Ti and Al. Coish and Taylor (1979) noted that some of the Ti-Al variation in Leg 34 pyroxenes result from rapid cooling of the margins of

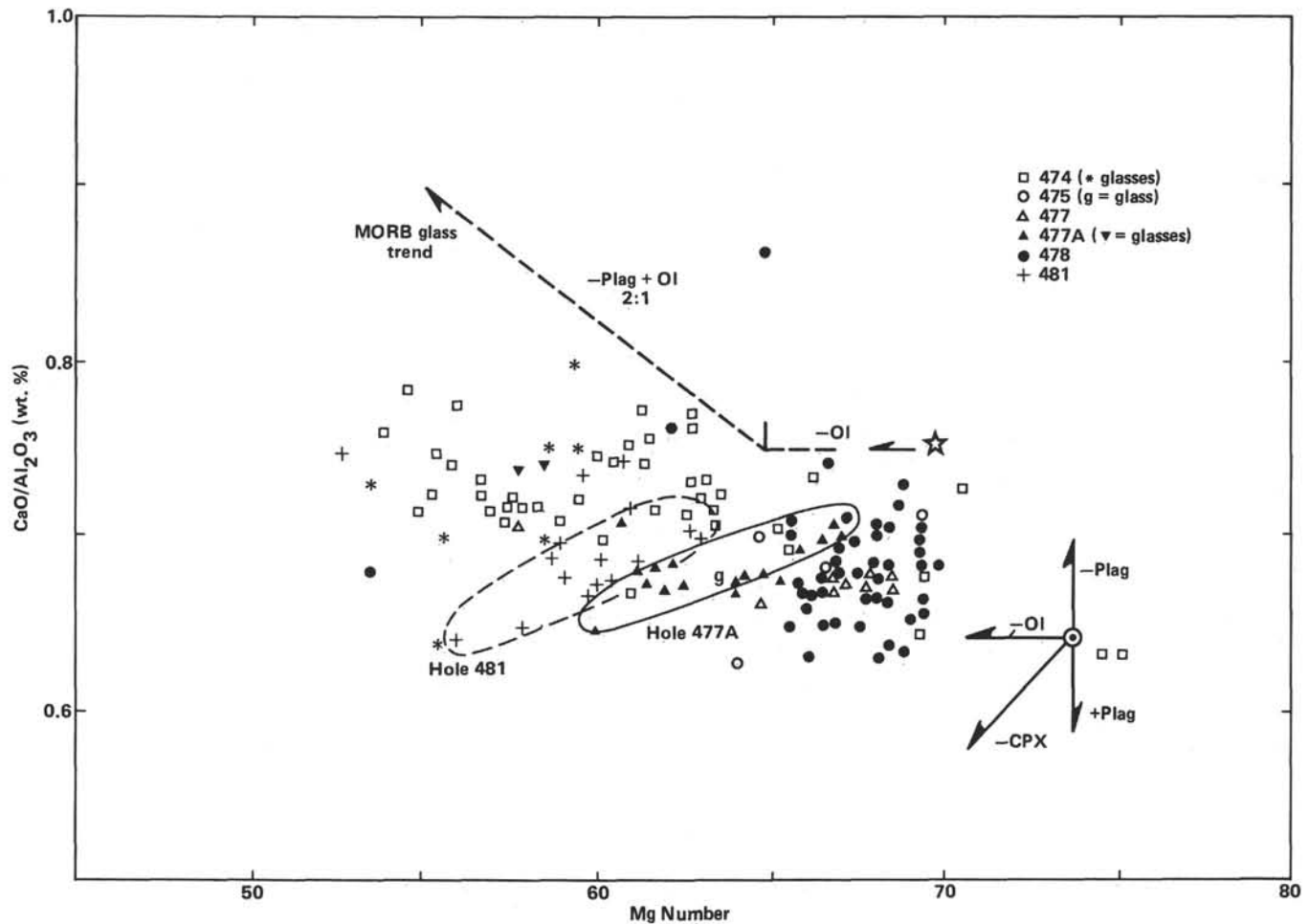


Figure 3.  $\text{CaO}/\text{Al}_2\text{O}_3$  versus Mg-number variation diagram, Leg 64 basalts. (Fractionation trends calculated for FAMOUS basalt, Section 472-1-1, indicated by the star, are shown [Bence, et al., 1979; see Fig. 1]. Note that natural-glass analyses of Leg 64 basalts [Fornari et al., this volume] are indicated. Generalized fractionation/accumulation trends are presented for Ol, Plag, and Cpx.)

basalt units versus slow cooling in the interior portions. It appears that cooling rate plays a more important role than does the changing liquid composition in Leg 64 pyroxenes, since the late-stage crystallization of groundmass plagioclase and titanomagnetite (which would deplete the Ti and Al content in residual liquids) has little effect on the high Ti-Al component in groundmass clinopyroxenes.

### Olivine

Olivine phenocrysts and microphenocrysts have limited compositional ranges within the samples (Table 5, Fig. 6). With the exception of a microphenocryst in dolerite from Section 478-42-2, the entire compositional range is from  $\text{Fo}_{88.2}$  to  $\text{Fo}_{83.4}$  (Fig. 6). Similar ranges have been reported in phenocrysts from basalts drilled during Leg 34 (Mazzullo and Bence, 1976). Assuming that the distribution of Fe and Mg between olivine and liquid can vary between  $K_d = 0.25$  and  $0.35$ , depending on the oxygen fugacity, temperature, and pressure during crystallization (see Walker et al., 1979; Bender et al., 1978), then it is likely that the olivines represent

near-liquidus phases that crystallized in equilibrium with magmas having compositions not significantly different from their present host basalts (Mg numbers ~60-65). Rhodes et al. (1979), however, note that an addition (accumulation) of 5%  $\text{Fo}_{90}$  to an evolved basalt with an Mg number of 56 will change it to a more primitive basalt (Mg number = 64) that only *appears* to be in equilibrium with the olivine.

### Opaque Minerals and Spinel

Titanomagnetite is a ubiquitous groundmass phase in basalts; however, only a few were analyzed for this initial study (Table 6). The ulvospinel component varies from ~75% in olivine-rich dolerite to ~52% in a coarse-grained dolerite, where it coexists with ilmenite. Based on the Buddington and Lindsley (1964) geothermometer, equilibration of ilmenite and titanomagnetite occurred at approximately  $1000^\circ\text{C}$  and  $\log f_{\text{O}_2} = -10.5$ . Similar values were reported for coexisting oxides in Leg 34 basalts (Mazzullo and Bence, 1976).

Chromium-aluminum spinel occurs as inclusions in olivine and/or microphenocrysts in the more mafic ba-

Table 3. Representative analyses of plagioclase, Holes 474A, 477, 478.

Mineral	Sample 474A-40-2, 38-40							Sample 474A-42-2, 20-23			Sample 474A-45-4, 7-9							
	1	2	3	4	5	6	7	8	9	10	11a	11b	11c	11e	11f	11g	11h	11i
SiO <sub>2</sub>	50.28	50.50	57.75	50.46	49.80	51.14	50.95	50.11	49.94	50.39	51.14	46.50	47.10	47.00	46.95	47.43	46.47	52.32
Al <sub>2</sub> O <sub>3</sub>	30.36	31.35	25.51	29.66	30.57	30.23	30.87	29.81	29.45	29.84	29.63	33.83	33.28	33.09	33.65	33.76	33.61	29.75
FeO <sup>+</sup>	0.49	0.40	0.45	0.73	0.41	0.36	0.52	0.54	0.41	0.33	1.10	0.31	0.30	0.26	0.29	0.33	0.32	0.53
MgO				0.27					0.21			0.55				0.23		
CaO	14.59	15.04	8.27	14.11	14.33	14.51	14.65	14.03	13.74	13.81	14.01	18.22	17.78	17.62	17.81	17.95	18.32	13.93
Na <sub>2</sub> O	3.56	3.29	6.96	3.41	3.56	3.27	3.22	3.17	3.32	3.61	3.3	1.03	1.24	1.23	1.05	1.42	1.10	3.84
K <sub>2</sub> O											0.08							
Total	99.27	100.57	98.95	98.63	98.66	98.51	100.21	97.66	97.07	97.99	99.81	99.98	99.70	99.20	99.75	101.01	99.82	100.36
Cations based on 32 oxygens																		
Si	9.262	9.178	10.454	9.345	9.222	9.364	9.277	9.351	9.370	9.367	9.363	8.570	8.685	8.704	8.647	8.625	9.579	9.494
Al	6.592	6.717	5.445	6.476	6.674	6.526	6.627	6.557	6.514	6.540	6.399	7.350	7.224	7.224	7.307	7.254	7.315	6.365
Fe	0.076	0.061	0.068	0.113	0.063	0.055	0.080	0.084	0.064	0.052	0.169	0.048	0.046	0.039	0.045	0.051	0.049	0.080
Mg				0.073					0.059			0.151				0.063		
Ca	2.879	2.928	1.605	2.799	2.843	2.846	2.858	2.805	2.762	2.752	2.751	3.600	3.512	3.496	3.515	3.505	3.623	2.709
Na	1.269	1.158	2.442	1.222	1.277	1.161	1.136	1.147	1.207	1.302	1.172	0.370	0.443	0.442	0.373	0.500	0.394	1.349
K											0.019							
Total	20.007	20.042	20.013	20.028	20.079	19.953	19.977	19.944	19.976	20.013	20.028	19.937	19.919	19.905	19.886	19.998	19.960	19.997
An	69.4	71.7	39.7	69.6	71.0	71.0	71.6	71.0	69.6	67.9	69.8	90.7	88.8	88.8	90.4	87.5	90.2	66.8

Note: Total Fe as FeO; blank means not detected. Analysis numbers: 1-7, intermediate to central points in groundmass microphenocrysts; 8-10, groundmass microphenocrysts; 11a-11e, rim to core of large megacryst; 11f-11i, core to rim of same megacryst; 12, groundmass microphenocryst. 13a-13f, rim to core of megacryst; 14-16, groundmass microcrystals; 23a-23d, rim to core of megacryst; 24-25, microphenocrysts; 26, microphenocryst. 17, phenocryst; 18a-18d rim to core of megacryst; 19-20, 22, phenocrysts; 21, groundmass; 29a-29b, core and rim of phenocryst enclosed in clinopyroxene; 30, core phenocryst; 31-34, cores of phenocrysts.

Table 3. (Continued).

12	Sample 474A-46-3, 80-82								Sample 474A-49-3, 146-149									
	13a	13b	13c	13d	13e	13f	14	15	16	23a	23b	23c	23d	24	25	26	17	18a
50.79	48.68	45.24	46.13	45.61	45.57	47.58	47.88	50.82	50.43	50.99	46.35	46.37	46.30	52.31	52.31	52.79	49.18	52.03
30.83	31.12	33.83	33.31	33.72	33.79	33.46	31.95	30.17	30.96	30.50	44.03	34.49	33.87	30.19	29.60	28.61	30.95	29.15
0.51	0.38	0.35	0.34	0.27	0.34	0.29	0.46	0.48	0.68	0.49	0.35	0.37	0.37	0.71	0.87	0.83	0.40	0.69
								0.25	0.24						0.33			
14.97	15.73	18.20	17.94	18.13	18.39	18.29	16.46	14.78	15.31	14.80	18.39	18.17	18.10	14.00	13.71	13.13	15.08	13.29
3.10	2.18	0.91	1.14	0.93	0.92	1.03	1.87	3.00	2.86	3.12	0.99	0.91	1.10	3.65	3.42	4.08	2.63	4.15
															0.13			
100.20	98.09	98.55	98.86	98.65	99.01	98.65	98.62	99.51	100.48	99.89	100.11	100.25	99.73	100.85	100.36	99.44	98.22	99.31
Cations based on 32 oxygens																		
9.246	9.074	8.460	8.593	8.516	8.489	8.521	8.903	9.318	9.185	9.313	8.532	8.511	8.511	9.450	9.494	9.659	9.144	9.544
6.617	6.837	7.458	7.316	7.421	7.420	7.375	7.004	6.522	6.646	6.568	7.384	7.463	7.375	6.430	6.335	6.172	6.783	6.304
0.077	0.059	0.005	0.053	0.042	0.054	0.045	0.071	0.074	0.103	0.075	0.054	0.048	0.057	0.107	0.132	0.127	0.061	0.106
								0.068	0.064						0.090			
2.921	3.142	3.647	3.580	3.627	3.671	3.663	3.280	2.904	2.988	2.896	3.628	3.573	3.582	2.709	2.666	2.574	3.003	2.613
1.092	0.788	0.331	0.411	0.335	0.333	0.374	0.675	1.067	1.011	1.103	0.354	0.325	0.393	1.278	1.205	1.448	0.946	1.476
															0.030			
19.972	19.901	19.968	19.954	19.941	19.967	19.978	19.932	19.954	19.997	19.954	19.952	19.920	19.958	19.974	19.953	19.979	19.937	20.042
72.8	79.9	91.7	89.7	91.5	91.7	90.7	82.9	73.1	74.7	72.4	91.1	91.7	90.1	67.9	68.4	64.0	76.1	63.9

Table 3. (Continued).

Sample 477-13-2, 145-146								Sample 478-42-2, 82-83					Sample 478-51-3, 52-53			
18b	18c	18d	19	20	21	22	27a	27b	28	29a	29b	30	31	32	33	34
46.44	45.87	46.25	50.47	50.10	51.21	46.80	52.45	60.43	49.94	53.85	53.77	53.13	55.14	57.31	54.59	56.02
33.63	33.71	33.77	30.57	30.81	30.22	33.99	29.53	24.57	30.99	28.61	28.80	29.17	27.92	26.82	28.48	26.92
0.18	0.27	0.31	0.40	0.46	0.70	0.31	0.51	0.66	0.35	0.47	0.52	0.47	0.51	0.48	0.50	0.49
18.08	18.08	17.97	14.56	15.05	14.04	17.94	13.07	6.96	15.22	12.24	12.43	12.74	11.66	9.82	12.17	10.28
1.12	1.14	1.22	3.41	3.09	3.60	1.00	4.09	6.86	2.43	4.73	4.73	4.37	5.01	5.82	4.74	5.52
								0.16								0.08
99.45	99.07	99.52	99.41	99.59	99.76	99.05	99.65	99.64	98.93	99.90	100.25	100.11	100.24	100.24	100.47	99.31
Cations based on 32 oxygens																
8.592	8.530	8.559	9.269	9.201	9.357	8.599	9.554	10.782	9.204	9.170	9.718	9.634	9.945	10.268	9.836	10.147
7.335	7.392	7.369	6.619	6.671	6.508	7.364	6.343	5.168	6.733	6.120	6.127	6.238	5.936	5.664	6.051	5.749
0.028	0.042	0.048	0.062	0.070	0.107	0.040	0.077	0.099	0.054	0.071	0.078	0.071	0.077	0.072	0.075	0.074
3.585	3.604	3.563	2.865	2.962	2.748	3.531	2.552	1.331	3.005	2.379	2.406	2.475	2.252	1.886	2.349	1.996
0.400	0.410	0.437	1.214	1.099	1.274	0.357	1.446	2.372	0.867	1.663	1.656	1.537	1.751	2.020	1.656	1.939
								0.036								0.018
19.94	19.978	19.975	20.029	20.022	19.994	19.897	19.972	19.813	19.863	20.002	19.995	20.016	19.962	19.910	19.966	19.924
90.0	89.8	89.1	70.2	72.6	68.3	90.8	63.8	35.6	77.6	58.9	59.2	61.7	56.3	48.3	58.7	50.5

salts recovered during Leg 64. Three representative analyses are presented in Table 7. They are characterized by relatively low Cr/Cr + Al ratios and high Mg/Mg + Fe<sup>2+</sup> ratios. They are compositionally most similar to the Al-rich spinels observed in some FAMOUS basalts (Fisk and Bence, 1980) and picrites from the Mid-Atlantic Ridge (Sigurdsson and Schilling, 1976). The experimental results of Fisk and Bence (1980) indicate that these Al-rich spinels may have crystallized from a Mg-rich liquid (similar to Sample 474A-42-1, 6 cm) at low pressure (1 atm.) or, alternatively, at higher pressures and temperatures > 1250°C.

### FRACTIONAL CRYSTALLIZATION MODELS

To test the hypothesis that some of the major- and trace-element variations in the basalts drilled during Leg 64 result from fractional crystallization and to determine quantitatively the proportions of the phases that could have been removed, a large number of fractional crystallization calculations were performed using a least-squares mixing program adapted from Wright and Doherty (1970) (Tables 8, 9). Whole-rock data were used as parental and derivative liquid compositions (Table 1);

consequently, possible inaccuracies may be attributed to the high phenocryst contents of some samples. The compositions of fractionated phases were taken from probe analyses of minerals in the least-fractionated samples from each hole. The program has the option of determining the best end-member composition for plagioclase and olivine. Thus, the computed An and Fo contents are given in Tables 8 and 9. The program can also determine whether a better fit is achieved by addition or by removal of a phase. In the few models where a negative sign appears in front of the mineral percentage, it means that the phase is in excess in the derivative liquid (i.e., crystal accumulation). With the exception of Models 1 and 14 (Table 8), the spinel composition used in the calculations was titanomagnetite rather than Cr-Al spinel. The "comments" column lists the oxides with the poorest computed "fit" (i.e., the largest percent difference between computed-parent and observed-parent composition), thus contributing substantially to the sum of the squares of residuals ( $\Sigma r^2$ ). A positive sign signifies that the oxide was calculated in excess in the parental liquid. The fact that K<sub>2</sub>O often results in a poor fit is not considered a serious problem, because it is so susceptible to secondary alteration.

Table 4. Representative clinopyroxene analyses, Holes 474A, 477, and 478.

Mineral	Analysis Number											
	Sample 474A-40-2, 38-40						474A-45-4, 7-9					
	1	2b	3	4	5	6	7	8	9	11	12	13
SiO <sub>2</sub>	48.76	48.59	47.80	46.47	47.33	47.63	47.99	49.32	48.02	49.35	49.72	49.45
Al <sub>2</sub> O <sub>3</sub>	3.55	4.41	5.07	5.52	5.80	5.95	5.68	3.08	4.85	3.49	4.56	4.67
TiO <sub>2</sub>	1.96	2.28	2.54	4.02	2.88	2.92	2.62	1.41	1.93	1.45	1.44	1.66
MgO	13.11	12.85	12.82	10.86	12.18	12.81	12.68	13.46	13.58	14.15	13.98	13.50
FeO	8.96	9.19	8.07	10.64	8.88	8.29	8.57	12.11	8.39	8.64	8.05	8.66
MnO	0.15	0.20	0.14	0.26	0.12	0.12	0.12	0.22	0.12	0.15	0.34	0.02
CaO	21.39	21.62	21.94	21.17	22.88	21.72	21.73	18.51	20.20	20.03	21.51	21.15
Na <sub>2</sub> O	0.52	0.63	0.43	0.55	0.41	0.64	0.63	0.40	0.00	0.00	0.40	0.00
Cr <sub>2</sub> O <sub>3</sub>	0.21	0.13	0.13	0.00	0.23	0.50	0.13	0.00	0.33	0.18	0.34	0.32
Total	98.61	99.90	98.94	99.49	100.71	100.58	100.15	98.51	97.42	97.44	100.34	99.62
Cations Based on 6.0 Oxygens												
Si	1.857	1.830	1.810	1.773	1.774	1.777	1.798	1.887	1.836	1.884	1.849	1.850
Al	0.143	0.170	0.190	0.227	0.226	0.223	0.202	0.113	0.164	0.116	0.151	0.150
ΣTET	2.000	2.000	2.000	2.000	2.000	2.000	2.000	2.000	2.000	2.000	2.000	2.000
Al <sup>vi</sup>	0.016	0.025	0.036	0.021	0.030	0.039	0.048	0.026	0.055	0.041	0.049	0.056
Ti	0.056	0.065	0.072	0.115	0.081	0.082	0.074	0.041	0.055	0.042	0.040	0.047
Mg	0.744	0.721	0.724	0.618	0.680	0.713	0.708	0.768	0.774	0.805	0.775	0.752
Fe	0.285	0.289	0.256	0.339	0.278	0.259	0.268	0.388	0.268	0.276	0.250	0.271
Mn	0.005	0.006	0.004	0.008	0.004	0.004	0.004	0.007	0.004	0.005	0.011	0.006
Ca	0.873	0.872	0.890	0.865	0.919	0.868	0.872	0.759	0.828	0.819	0.857	0.848
Na	0.038	0.046	0.032	0.041	0.030	0.046	0.046	0.030	0.000	0.000	0.029	0.000
Cr	0.006	0.004	0.004	0.000	0.007	0.015	0.004	0.000	0.010	0.005	0.010	0.010
ΣCations	4.024	4.029	4.018	4.008	4.029	4.026	4.024	4.018	3.994	3.993	4.020	3.989
En	39.0	38.2	38.6	33.7	36.2	38.7	38.2	40.0	41.3	42.3	40.9	40.2
Fs	15.2	15.6	13.9	19.0	15.0	14.2	14.7	20.5	14.5	14.7	13.8	14.5
Wo	45.8	46.2	47.5	47.3	48.8	47.1	47.1	39.5	44.2	43.0	45.3	45.3
Quad	92.3	90.8	88.8	86.4	88.4	86.6	87.5	93.4	89.1	92.5	90.2	90.1
Others	7.7	9.2	11.2	13.6	11.6	13.4	12.5	6.6	10.9	7.5	9.8	9.9
Mg/Mg + Fe	0.723	0.714	0.739	0.645	0.710	0.734	0.725	0.665	0.743	0.745	0.756	0.735

Note: All Fe as FeO; 1-7, clinopyroxenes in groundmass, interstitial grains; 8-11, groundmass clinopyroxene; 12-13, subophitic; 14-15, clinopyroxene crystals; 19-25, subhedral subophitic grains; 27, larger phenocryst partially enclosing 26; 28-29, ophitic phenocrysts; Rim (30A) and core (30B) of single grain.

**Hole 474A**

The suite of Hole 474A basalts exhibits a wide range of chemical compositions and a significant degree of differentiation. Variations in CaO/Al<sub>2</sub>O<sub>3</sub> with Mg number (Fig. 3) suggest strong Ol + Plag control of fractionation. Saunders et al. (this volume) suggest that olivine and spinel accumulation may account for the high MgO, Cr, and Ni in picritic basalts such as those from Samples 474A-42-1, 6 cm and 474A-40-1, 19 cm. Model 1 suggests that an olivine-rich dolerite (Sample 474A-40-2, 40 cm) could be derived from picrite by Ol + Spnl fractionation or, alternatively, that the picrite contains about 15% cumulate olivine + spinel. Similarly, the derivation of a more typical basalt (Sample 474A-39-3, 148 cm) from picrite or olivine-rich dolerite (Models 2, 15, 16) requires the removal of large percentages of olivine (Fo<sub>90</sub>). Considering the heterogeneous distribution of olivine phenocrysts in Units 1 and 2, it is likely that the picritic lavas are, in part, cumulate. Smaller percentages of plagioclase ± clinopyroxene ± spinel must also be removed, however, to generate more fractionated basalts, suggesting that olivine subtraction or accumulation alone cannot explain the major-element trends.

Petrographic evidence indicates that Plag + Ol ± Cr-spinel are near-liquidus phases in the more mafic basalts and should control the early liquid line of descent. Models 4 and 12 indicate that this scheme, with approximately 2 parts Plag to 1 part Ol, is fairly successful. In comparison to Model 4, however, Model 5 results in a better fit (lower Σr<sup>2</sup>) when Cpx is included as a fractionating phase. In fact, in deriving the more evolved rocks (Samples 474A-50-3, 91 cm, 474A-50-4, 1 cm, 474A-49-2, 31 cm), Cpx fractionation is essential (see Models 5-11, 17). Clinopyroxene fractionation must have occurred at higher pressures (deeper depths), according to the experimental work of Bender et al. (1978), and there is little petrographic evidence for this occurrence, because no Cpx phenocrysts occur in the Hole 474 rocks. Plagioclase continues to dominate the fractionating assemblage, which explains the rapid decrease in Al<sub>2</sub>O<sub>3</sub> with MgO in Figure 1.

The calculations support the proposals of Saunders et al. (this volume) that basalts from Units 6, 7, and 8 can be related by fractional crystallization of Plag + Ol + Cpx from the same or a similar parental magma. Since the proportions of fractionating minerals are so variable, however, the calculations suggest that the basalts are not all related by the same liquid line of de-

Table 4. (Continued).

Sample 477-13-2, 145-146		Sample 478-42-2, 82-83										Sample 478-51-3, 52-53			
14	15	19	20	21	22	23	24	25	26	27	28	29	30A	30B	
48.95	49.96	51.71	51.78	51.07	51.37	52.94	51.21	52.55	51.85	52.02	51.41	51.75	51.29	51.96	
5.06	5.02	2.86	2.69	3.49	3.30	2.17	3.72	1.89	2.28	2.39	2.40	1.99	2.70	2.62	
2.25	2.13	0.92	0.88	0.87	0.80	0.53	0.81	0.58	1.34	1.29	1.39	0.98	1.24	0.97	
13.06	13.50	15.59	15.90	15.81	15.72	17.14	16.10	16.37	14.29	14.92	14.66	15.61	15.42	15.65	
8.74	8.47	7.00	6.91	6.78	5.64	5.00	5.00	6.48	9.06	8.46	9.00	8.42	7.49	7.26	
0.14	0.14	0.18	0.12	0.16	0.14	0.19	0.00	0.00	0.19	0.12	0.19	0.22	0.18	0.23	
21.02	21.60	21.23	21.05	20.78	21.45	20.93	21.87	21.32	20.90	20.66	20.82	19.75	20.98	21.35	
0.40	0.00	0.51	0.50	0.54	0.41	0.45	0.55	0.00	0.00	0.00	0.41	0.64	0.00	0.00	
0.27	0.33	0.23	0.14	0.50	0.42	0.34	0.51	0.14	0.00	0.17	0.00	0.13	0.13	0.00	
99.89	100.15	100.23	99.97	100.00	99.25	99.69	99.77	99.33	99.91	100.03	100.28	99.49	99.43	100.04	
Cations Based on 6.0 Oxygens															
1.832	1.826	1.908	1.913	1.887	1.904	1.941	1.885	1.945	1.930	1.927	1.911	1.930	1.908	1.919	
0.168	0.174	0.092	0.087	0.113	0.096	0.059	0.115	0.055	0.070	0.073	0.089	0.070	0.092	0.091	
2.000	2.000	2.000	2.000	2.000	2.000	2.000	2.000	2.000	2.000	2.000	2.000	2.000	2.000	2.000	
0.055	0.047	0.032	0.030	0.039	0.048	0.035	0.047	0.027	0.030	0.032	0.016	0.017	0.027	0.033	
0.063	0.060	0.026	0.024	0.024	0.022	0.015	0.022	0.016	0.038	0.036	0.039	0.027	0.035	0.027	
0.728	0.751	0.857	0.875	0.871	0.868	0.937	0.884	0.903	0.793	0.824	0.812	0.868	0.855	0.861	
0.273	0.264	0.216	0.213	0.210	0.175	0.153	0.154	0.201	0.282	0.262	0.280	0.263	0.233	0.224	
0.004	0.004	0.006	0.004	0.005	0.004	0.006	0.000	0.000	0.006	0.004	0.006	0.007	0.006	0.007	
0.843	0.863	0.839	0.833	0.823	0.852	0.822	0.863	0.845	0.834	0.820	0.829	0.789	0.836	0.845	
0.029	0.000	0.036	0.036	0.039	0.029	0.032	0.039	0.000	0.000	0.000	0.030	0.046	0.000	0.000	
0.008	0.010	0.007	0.004	0.015	0.012	0.010	0.015	0.004	0.000	0.005	0.000	0.004	0.004	0.000	
4.004	3.999	4.019	4.020	4.025	4.011	4.009	4.024	3.996	3.982	3.982	4.012	4.012	3.996	3.997	
39.4	39.8	44.7	45.5	45.6	45.7	48.8	46.5	46.3	41.4	43.1	42.2	45.0	44.3	44.5	
15.0	14.3	11.6	11.3	11.2	9.5	8.3	8.1	10.3	15.1	13.9	14.8	14.0	12.4	11.9	
45.6	45.9	43.7	43.3	43.1	44.8	42.9	45.4	43.4	43.5	42.9	43.0	41.0	43.3	43.6	
87.4	88.6	93.6	94.2	92.3	91.8	94.1	91.7	96.0	96.1	96.2	94.5	95.2	94.3	94.5	
12.6	11.4	6.4	5.8	7.7	8.2	5.9	8.3	4.0	3.9	3.8	5.5	4.8	5.7	5.5	
0.727	0.740	0.799	0.804	0.806	0.832	0.859	0.852	0.818	0.738	0.759	0.744	0.768	0.786	0.793	

Table 5. Representative analyses of olivine, Hole 474A, 475B, 477, and 478.

Mineral	Analysis Number		Sample 474A-42-2, 20-23					Sample 475B-2-1, 0-9					Sample 474A-46-3, 80-82					Sample 477-13-2, 145-146			Sample 478-42-2, 82-83
	1a	1b	2	3a	3b	4	5	6	8	10	11	12	13	14	15	16	18	19	20	22	
SiO <sub>2</sub>	40.00	40.58	39.93	40.20	39.83	40.11	40.51	39.87	40.34	40.21	40.26	39.48	40.75	40.05	40.11	40.16	39.17	40.14	39.91	38.09	
FeO	11.30	11.67	11.64	11.57	11.57	11.62	11.22	11.99	11.25	12.21	11.43	14.20	11.25	13.28	14.28	13.76	15.53	15.27	15.32	26.00	
MnO	0.13	0.16	0.18	0.12	0.20	0.17	—	0.18	0.15	0.15	—	0.18	0.15	0.17	0.15	0.17	0.15	0.24	0.26	0.41	
MgO	46.49	46.85	46.71	46.98	46.82	46.82	46.88	45.71	47.00	45.44	46.70	44.69	47.09	44.51	45.54	45.01	43.89	44.27	43.90	35.18	
CaO	0.27	0.27	0.26	0.38	0.35	0.24	0.37	0.37	0.39	0.33	0.39	0.38	0.39	0.40	0.39	0.35	0.37	0.38	0.35	0.29	
NiO	0.17	0.22	0.27	0.22	0.27	0.30	0.32	0.27	0.24	0.23	0.15	—	0.23	0.21	0.16	0.21	—	—	0.16	—	
Total	98.34	99.75	98.99	99.46	99.04	99.27	99.29	98.38	99.35	98.56	98.92	99.81	99.86	98.61	100.63	99.67	99.12	100.34	99.90	100.20	
Cations Based on 4 Oxygens																					
Si	1.005	1.006	0.999	1.000	0.997	1.001	1.007	1.001	1.002	1.012	1.002	1.000	1.007	1.012	0.998	1.006	0.996	1.003	1.005	1.006	
Fe	0.237	0.242	0.244	0.241	0.242	0.242	0.233	0.252	0.234	0.257	0.238	0.301	0.233	0.281	0.297	0.288	0.330	0.319	0.323	0.575	
Mn	0.003	0.004	0.004	0.002	0.004	0.004	—	0.004	0.003	0.003	—	0.004	0.003	0.004	0.003	0.004	0.003	0.005	0.006	0.009	
Mg	1.740	1.731	1.742	1.742	1.746	1.740	1.737	1.710	1.740	1.703	1.733	1.686	1.735	1.676	1.689	1.681	1.664	1.649	1.648	1.385	
Ca	0.007	0.007	0.007	0.010	0.009	0.006	0.010	0.010	0.010	0.009	0.010	0.010	0.010	0.011	0.010	0.009	0.010	0.010	0.009	0.008	
Ni	0.003	0.004	0.005	0.004	0.005	0.006	0.006	0.005	0.005	0.005	0.003	—	0.005	0.004	0.003	0.004	—	—	0.003	—	
Total	2.995	2.994	3.001	3.000	3.003	2.999	2.993	2.981	2.995	2.988	2.986	3.000	2.993	2.988	3.002	2.993	3.004	2.986	2.995	2.990	
Fo	88.0	87.7	87.7	87.9	87.8	87.7	88.2	87.2	88.2	86.9	87.9	84.9	88.2	85.7	85.0	85.4	83.4	83.8	83.6	70.7	

Note: All Fe as FeO; blank means not detected. 1a–1b, core and rim of microphenocryst; 2, core of microphenocryst; 3a–3b, core and rim of phenocrysts; 4, 5, interiors of phenocrysts; 6, 8, microphenocrysts; 10, 11, phenocrysts; 12, 14, 15 microphenocrysts; 13, 16 phenocrysts; 18, 20 microphenocrysts, 19 phenocryst; 22 small anhedral phenocryst.

Table 6. Representative analyses of iron–titanium oxides, Holes 474A and 478.

Mineral	Analysis Number		Sample 474A-40-2, 38-40			Sample 474A-45-4, 45-4, 7-9		Sample 478-51-3, 52-53		
	1	2	3	5	6	7	8	9		
SiO <sub>2</sub>	1.10	1.42	0.81	2.39	2.62	0.69	0.64	0.70		
Al <sub>2</sub> O <sub>3</sub>	2.28	2.17	1.94	2.42	1.97	0.85	0.00	2.06		
TiO <sub>2</sub>	24.97	25.95	25.71	20.36	22.56	18.01	50.02	18.34		
Fe <sub>2</sub> O <sub>3</sub>	16.30	13.45	15.82	18.28	16.00	31.28	6.31	29.18		
FeO	51.91	52.86	52.84	50.94	54.31	45.62	38.46	44.68		
MgO	2.28	2.06	1.89	0.41	0.36	1.46	3.66	2.55		
MnO	0.63	1.14	0.64	0.50	0.47	0.56	0.62	0.52		
CaO	0.12	0.15	0.00	0.18	0.15	0.10	0.10	0.00		
V <sub>2</sub> O <sub>5</sub>	0.70	0.60	0.49	0.48	0.59	0.52	0.30	1.16		
Total	100.29	99.80	100.14	95.96	99.03	99.09	100.11	99.19		
% Oliv.	70.8	74.8	72.6	64.3	69.6	52.0	88.3	52.1		
Cations Based on 32 Oxygens										
Si	0.319	0.413	0.236	0.730	0.777	0.207	0.126 <sup>a</sup>	0.206		
Al	0.778	0.744	0.667	0.872	0.688	0.300	0.000	0.716		
Ti	5.438	5.676	5.639	4.679	5.030	4.058	7.385	4.065		
Fe <sup>3+</sup>	3.552	2.944	3.472	4.204	3.570	7.052	0.932	6.472		
Fe <sup>2+</sup>	12.572	12.859	12.889	13.018	13.465	11.430	6.315	11.014		
Mg	0.984	0.893	0.882	0.187	0.159	0.652	1.070	1.120		
Mn	0.155	0.281	0.158	0.129	0.118	0.142	0.103	0.130		
Ca	0.037	0.047	0.000	0.059	0.048	0.032	0.021	0.000		
V	0.163	0.140	0.115	0.118	0.140	0.125	0.047	0.274		
Total	24.00	24.00	24.00	24.00	24.00	24.00	16.00	24.00		

Note: Fe<sub>2</sub>O<sub>3</sub> calculated on the basis of ideal spinel stoichiometry: 1–3, subhedral intersertal; 5–6, groundmass crystals; 7–9 groundmass grains.

<sup>a</sup> Based on 24 oxygens.

scent. Certainly, the inhomogeneous distribution of phenocrysts and the presence of plagioclase xenocrysts in some samples (i.e., high Al<sub>2</sub>O<sub>3</sub> basalts in Sample 474A-47-1, 101 cm) complicate these simple models. Although Units 1 and 2a can be related by fractional crystallization, no combination of mineral extracts from these basalts yielded reasonable solutions for deriving the more fractionated basalts in the underlying units—a point that supports the hypothesis of at least two distinct magma batches at this site.

### Hole 475B

Least-squares fractionation calculations for Hole 475 basalts indicate that the samples could be related to a single parental magma (Sample 475B-4-1, 2 cm) by Plag + Ol + Cpx fractionation (see Models 18–20, Table 8). The percentages of derivative liquid remaining after fractional crystallization are reasonable (74–86%) and the residuals are small ( $\Sigma r^2 < 0.08$ ) in Models 18 and 20. In these models, olivine must become more fayalitic and

Table 7. Representative spinel analyses from Hole 474A.

Mineral	Analysis Number		Sample 474A-42-2, 20-23		
	1	2	3		
SiO <sub>2</sub>	0.67	3.73	0.87		
TiO <sub>2</sub>	0.29	0.65	0.34		
Al <sub>2</sub> O <sub>3</sub>	40.23	34.82	42.37		
V <sub>2</sub> O <sub>5</sub>	0.14	0.17	0.13		
Cr <sub>2</sub> O <sub>3</sub>	25.85	23.55	21.97		
Fe <sub>2</sub> O <sub>3</sub>	2.44	2.00	3.34		
FeO	11.58	16.62	12.25		
Mg	17.90	15.99	17.85		
MnO	0.14	0.29	0.26		
CaO	0.16	0.95	0.11		
NiO	0.26	0.18	0.18		
Total	99.66	98.95	99.67		
Cr/Cr + Al	0.301	0.312	0.258		
Mg/Mg + Fe <sup>2+</sup>	0.734	0.632	0.723		
Fe <sup>3+</sup> /Cr + Al + Fe <sup>3+</sup>	0.026	0.025	0.036		

Note: 1, groundmass euhedral grain; 2–3, subhedral inclusions in olivine. Fe<sub>2</sub>O<sub>3</sub> calculated assuming ideal spinel stoichiometry.

plagioclase more albitic as fractionation proceeds. The absence, as in the holes already mentioned, of modal plagioclase and clinopyroxene, however, is problematic. Only 5–10% Ol with traces of spinel exists in these glassy basalts, yet significant amounts of Plag and Cpx fractionation are predicted to explain the major-element variations at this site. Furthermore, the relatively constant Ni, Cr, and incompatible trace-element contents in these samples suggest that little crystallization of Ol or Cpx could have occurred.

### Holes 477 and 477A

Results of the fractionation calculations for basalts from the Guaymas Basin are presented in Table 9. In general, the dolerites from Hole 477 are plagioclase-rich with correspondingly high Al<sub>2</sub>O<sub>3</sub> and Sr contents (see Fig. 1). On the basis of trace-element abundances, Saunders et al. (this volume) have suggested that Units 2b

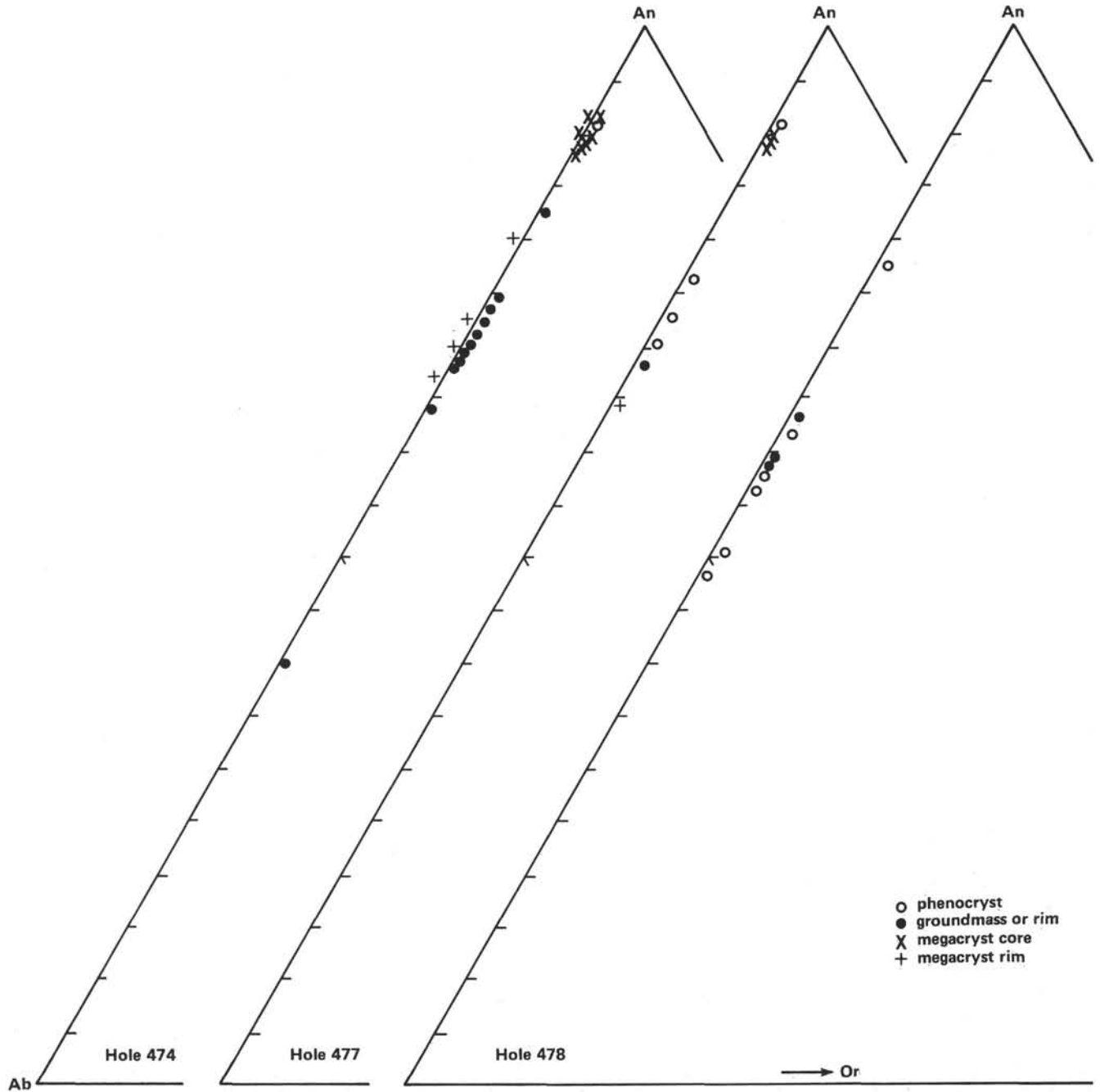


Figure 4. Ternary plot of Or-Ab-An end members for plagioclases in basalts, Holes 474, 477, and 478. (Open symbols represent phenocrysts; closed symbols represent groundmass or rim compositions. Note that megacryst [often xenocrysts] rims and cores are also plotted.)

and 2c could have been derived from the same parental magma by low-pressure fractional crystallization of approximately 30% Plag + Ol. Our calculations indicate that the removal of 11.5 wt.% Ol and 15.3 wt.% Plag from a magma with the composition of Sample 477-12-4, 76 cm (Mg number: 68.32) would result in 72.3% liquid with a composition like that in Sample 477-9-1, 57 cm (Model 3, Table 9). Slight intraunit variations can also be explained by Ol + Plag ± Cpx fractionation (see Models 1, 2, 4, 5). The addition of small percentages of Cpx as a fractionating phase improves the least-squares fit (compare Models 1 and 2, 4 and 5).

In Hole 477A, olivine (5%) and plagioclase (5%) appear to be the only liquidus phases in the quenched upper chill zone, but plagioclase and clinopyroxene with lesser olivine are the predominant modal phases down-hole, as the basalt changes to dolerite and gabbro. The high Al<sub>2</sub>O<sub>3</sub> contents almost certainly reflect the high modal plagioclase abundance, and a slight positive europium anomaly in one sample (Saunders et al., this volume) suggests plagioclase accumulation.

Chemical data strongly suggest that the units from Holes 477 and 477A could have been derived from a common parental magma involving varying degrees of

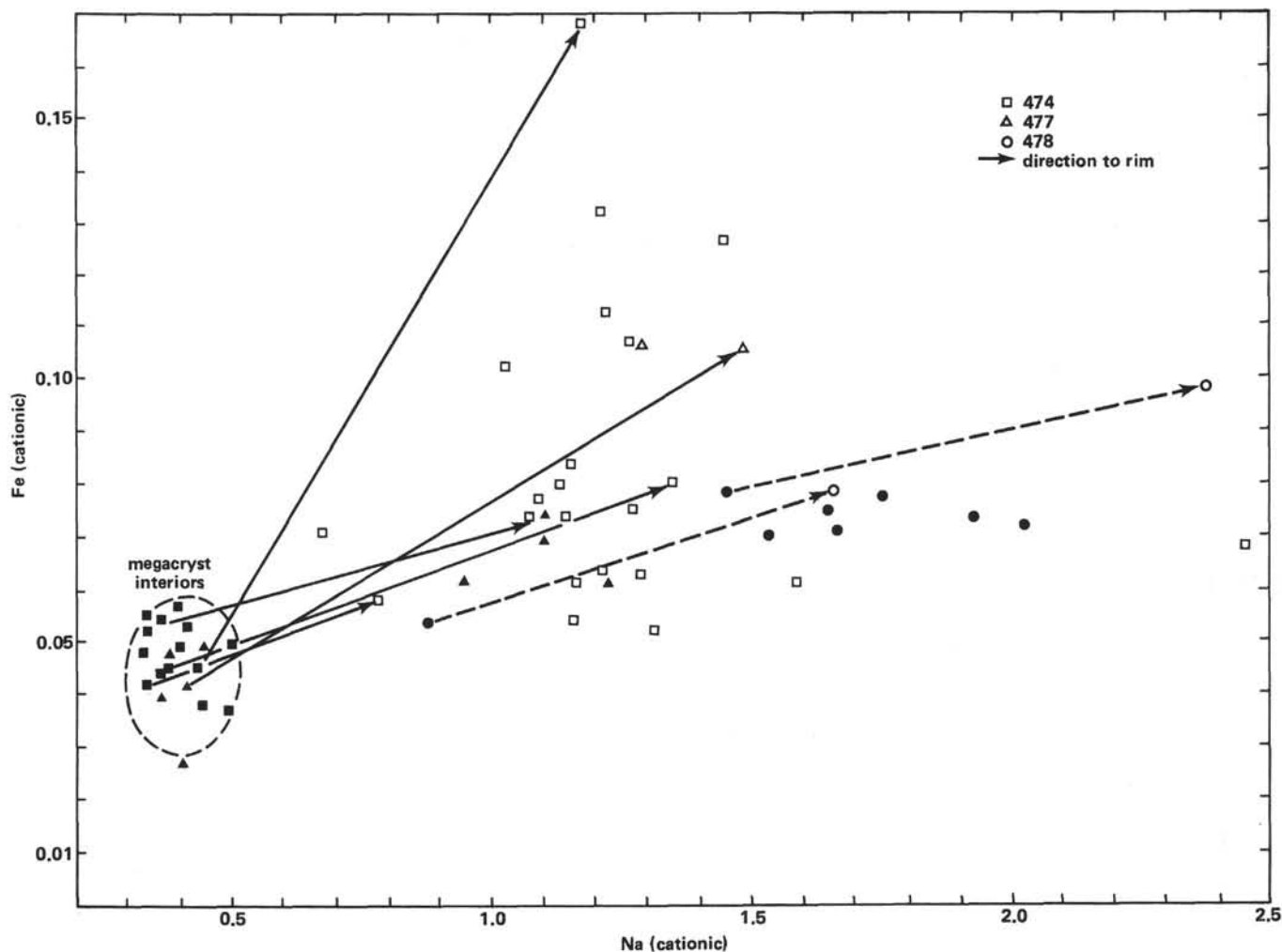


Figure 5. Plot of molecular abundance of Fe versus Na (based on 32 oxygens) for plagioclases, Sites 474, 477, and 478. (Phenocryst and megacryst cores and interior portions are indicated by solid symbols. Rims and groundmass plagioclase are open symbols. Solid lines connect individual cores and rims of megacrysts. Dashed lines connect cores and rims of phenocrysts.)

Ol + Plag fractionation (Saunders et al., this volume). Model 7 indicates that Ol + Plag (1:1) fractionation is a viable mechanism, but Model 8 shows that the removal of nearly equal percentages of Cpx + Ol + Plag gives a better result. The derivation of high-alumina basalts in Hole 477A also requires Cpx + Ol + Plag fractionation (Model 10). An even better fit, however, is obtained in Model 11 by removing Ol  $\pm$  Cpx from parental basalt Sample 477A-12-4, 76 cm and accumulating a small amount (5.47 wt.%) of plagioclase in the derivative liquid to produce high-alumina basalt in Sample 477A-3-21, 17 cm.

The need to include clinopyroxene as a fractionating phase in the differentiation scheme at Hole 477 is similar to that in the holes previously discussed. Perhaps the best evidence for the involvement of clinopyroxenes is the presence of clinopyroxene phenocrysts in some of the coarser-grained rocks in Hole 477 and the clinopyroxene-rich gabbroic regions observed in Hole 477A. Decreasing CaO/Al<sub>2</sub>O<sub>3</sub> ratios with differentiation clearly imply that clinopyroxene may have been removed; but in cases where plagioclase addition has also oc-

curred, a similar decrease will also occur (see Fig. 3 and Sample 13-2, 17 cm).

#### Hole 478

Constant incompatible element ratios and similar chemical compositions of basalts from Units 4, 5, and 6 suggest that these intrusives are consanguineous (Saunders et al., this volume). The most successful calculations indicate that Cpx + Plag + Ol could be fractionated from mafic basalts (Mg numbers  $\sim$  69) in relatively constant weight proportions (Cpx:Plag:Ol = 2:8:3) to generate the differentiated basalts in Units 4 through 6. As in previous models, better results (lower  $\Sigma r^2$ ) were obtained with a three-phase assemblage rather than with only Ol + Plag (compare Models 16 and 17). When clinopyroxene is involved, however, relatively greater percentages of crystals (> 50%) must be removed, and the compositions of plagioclase and olivine are unlike observed phenocryst compositions. Therefore, low-pressure crystallization of Ol + Plag may be more realistic in this case.

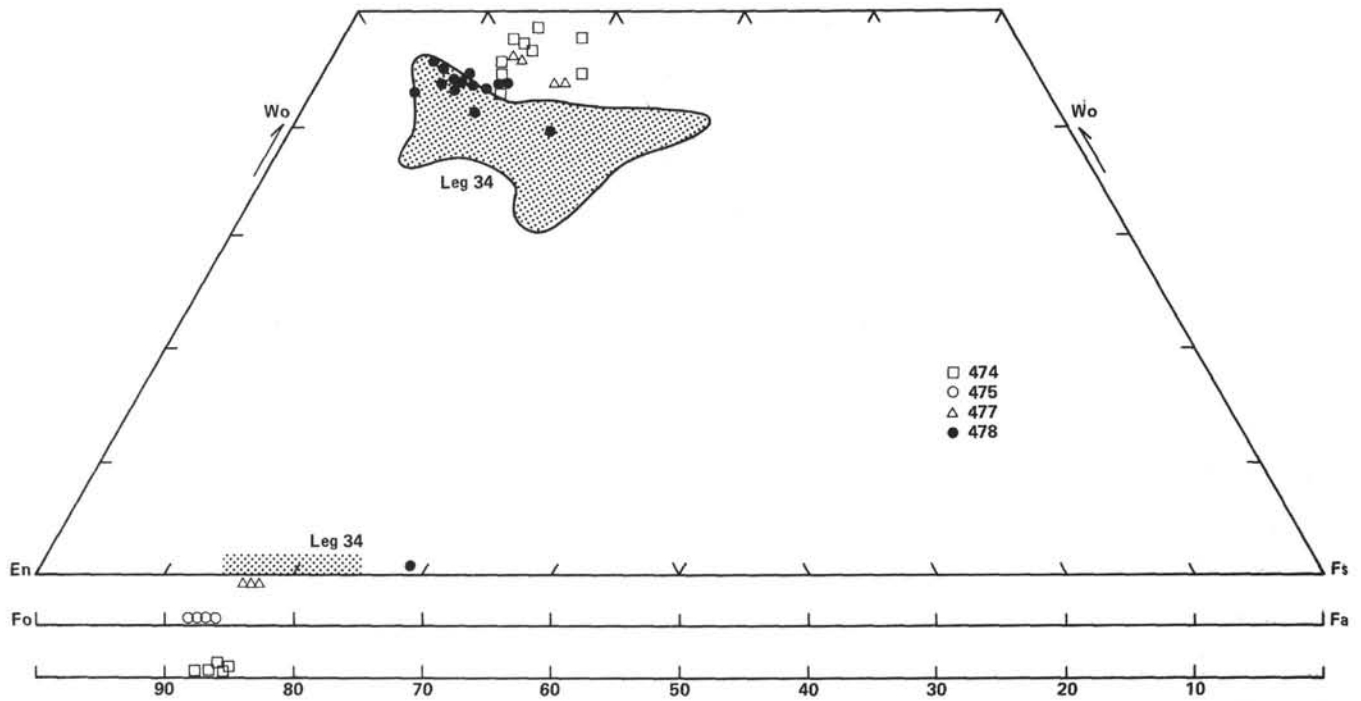


Figure 6. Pyroxene analyses (see Table 4) plotted on the pyroxene quadrilateral (Ca-Mg-Fe + Mn). (Olivine compositions [see Table 5] are also plotted on the base of the quadrilateral along the Mg-Fe join. Fields [stippled pattern] for pyroxenes in basalts from Leg 34 [Mazzullo and Bence, 1976] are shown for comparison.)

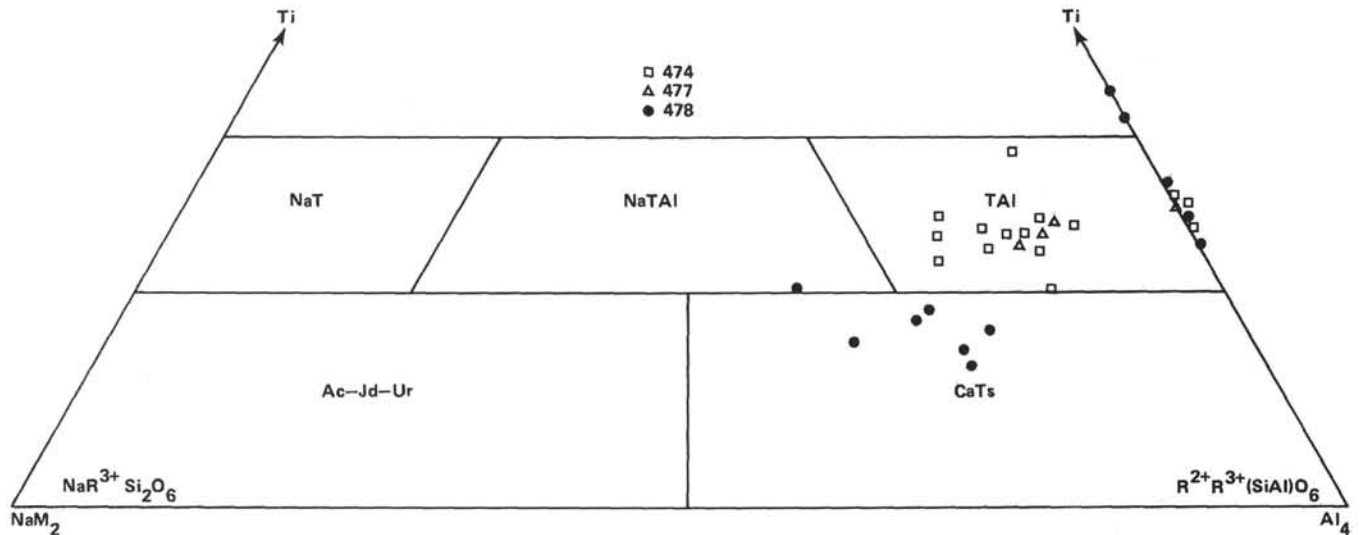


Figure 7. Pyroxene quadrilateral showing "other" components in pyroxenes, Holes 474, 477, and 478.

A xenolith of differentiated gabbro (Sample 478-51-3, 49 cm) highly enriched in incompatible elements may be derived by extensive fractionation (66–82%) of a mafic parent. Low MgO, Ni, and Cr contents, high incompatible-element abundances, a negative europium anomaly, and low Ti/Zr ratios led Saunders et al. (this volume) to suggest removal of Ol + Cpx + Plag + ilmenite ± titanomagnetite from a melt at the top of a subridge magma chamber to produce the composition of the xenolith. Model 15 (Table 9) supports this but indicates that >80% of the original magma would have

had to crystallize. Such extensive crystallization would severely deplete residual liquids in Ni and Cr and cause four- to tenfold enrichments in incompatible elements. With the deletion of titanomagnetite as a fractionating phase, the fit is not as good, but the percentages of residual liquids (~33%) are in better agreement with the observed trace-element abundances in the gabbro.

As was found for Hole 477, there is some petrographic evidence that support Cpx extraction in Hole 478. Clinopyroxene and plagioclase are cumulate phases in some of the coarse-grained rocks of Cores 42 and

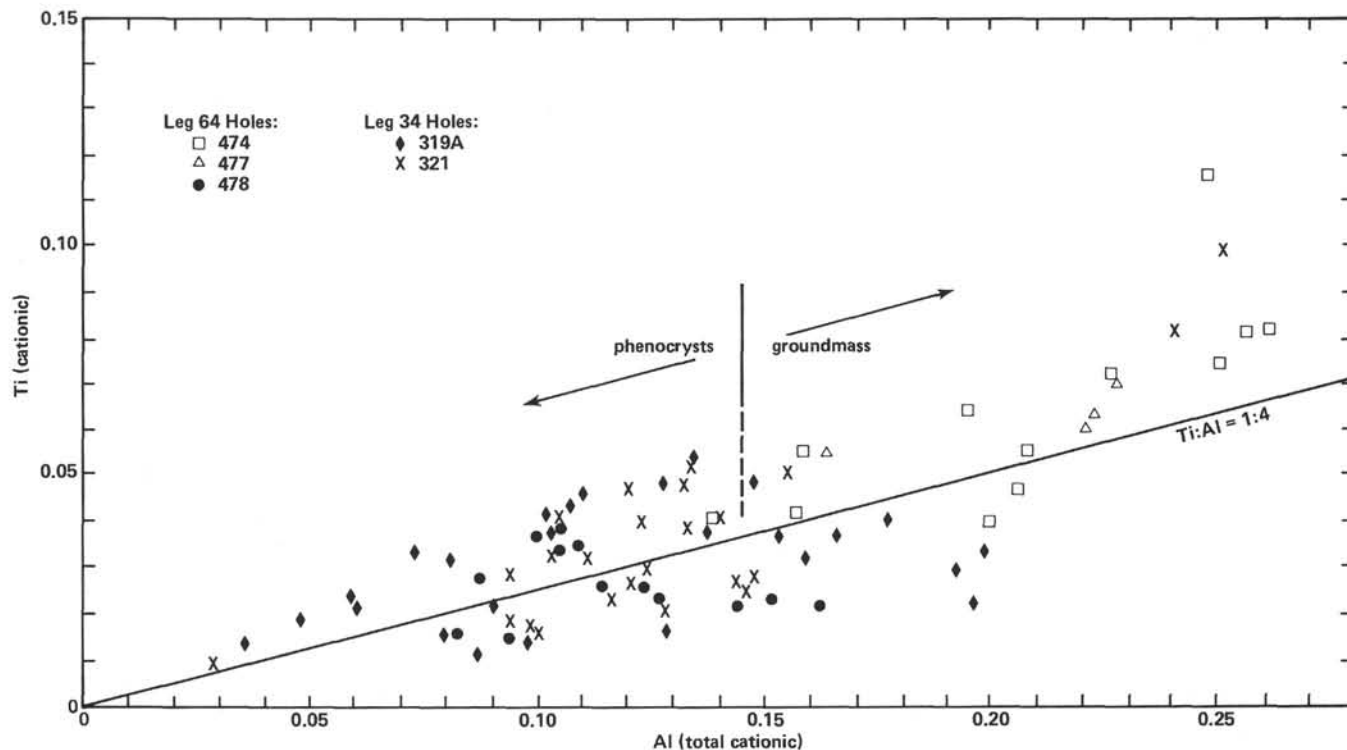


Figure 8. Plot of molecular Ti versus Al (total) in pyroxenes. (Substitutional trend of 1 Ti:4 Al molecules is shown. Generalized fields of phenocrysts and groundmass pyroxenes are defined. Analyses of pyroxenes from Leg 34 [Holes 319A and 321; Mazzullo and Bence, 1976] are plotted for comparison to pyroxenes from Leg 64.)

43, and clinopyroxene may be enclosed in plagioclase, which suggests it was a near-liquidus phase. In general, olivine comprises only a small modal percentage of these basalts (5%), whereas clinopyroxene may constitute 20 to 50% of the mode.

#### Hole 481A

The suite of basalts recovered from Hole 481A is, as a whole, the most evolved in the Guaymas Basin. The samples have low  $\text{Al}_2\text{O}_3$  contents (Fig. 1) and most show a negative correlation between  $\text{CaO}/\text{Al}_2\text{O}_3$  and Mg number (Fig. 3). As in Holes 477 and 478, the basalts are transitional from glassy and vitrophyric to doleritic and gabbroic in the centers of intrusive units. The most evolved sample is a gabbro (Sample 481A-15-3, 115 cm) in the center of a subunit.

Fractionation models stress the dominance of Cpx + Plag fractionation in Unit 1 (Models 21-23, Table 9). Little variation in Ni abundances with increasing Zr contents suggests that olivine fractionation was not significant during differentiation (Saunders et al., this volume). Our calculations confirm this suggestion. However, in deriving low MgO basalt (Sample 481-33-1, 91 cm) in Unit 3 from a more mafic parent, such as Sample 481-17-2, 6 cm) in Unit 1, 9.6% Plag + 6.3% Ol, and only minor Cpx (0.3%) need be removed (Model 24, Table 9). This scheme explains the low Ni and high  $\text{CaO}/\text{Al}_2\text{O}_3$  ratio in the residual liquid.

#### Intersite Relations

It is likely that the mantle sources for basalts at Sites 478 and 481 are chemically distinct from the source of

basalts at Site 477 (Saunders et al., this volume). Models 25 and 26 (Table 9) suggest that it is possible to derive basalts from Hole 481A (Samples 481A-15-3, 27 cm, 481A-17-2, 6 cm) by ~60% fractional crystallization of a parental magma with the composition of Sample 478-49-1, 63 cm. As within each hole, plagioclase dominates the fractionated assemblage, and Ol + Cpx are removed in near-equal amounts.

#### DISCUSSION

Major-element, trace-element, and mineralogic data from basalts drilled during Leg 64 indicate that a wide chemical variety of N-type MORB has been erupted in the Gulf of California. In particular, the Leg 64 basalts have chemical and mineralogical characteristics broadly similar to those from the East Pacific Rise and the Nazca Plate, although they are not nearly so evolved as many of the basalts from the Galapagos Spreading Center (see Mazzullo and Bence, 1976; Clague and Bunch, 1976; Byerly, 1980; Perfit et al., 1980; Saunders et al., this volume).

The trace-element data indicate that a number of distinct N-type mantle sources or a fairly heterogeneous mantle was partially melted to generate the spectrum of basalts recovered during Leg 64. Regular variations in both major- and trace-element abundances with increased fractionation appear to be a consequence of closed-system fractional crystallization. Although the least-squares models we have presented generally support this assumption, close examination of the mathematical results with respect to the phase relations in the samples, experimental data on MORB crystallization,

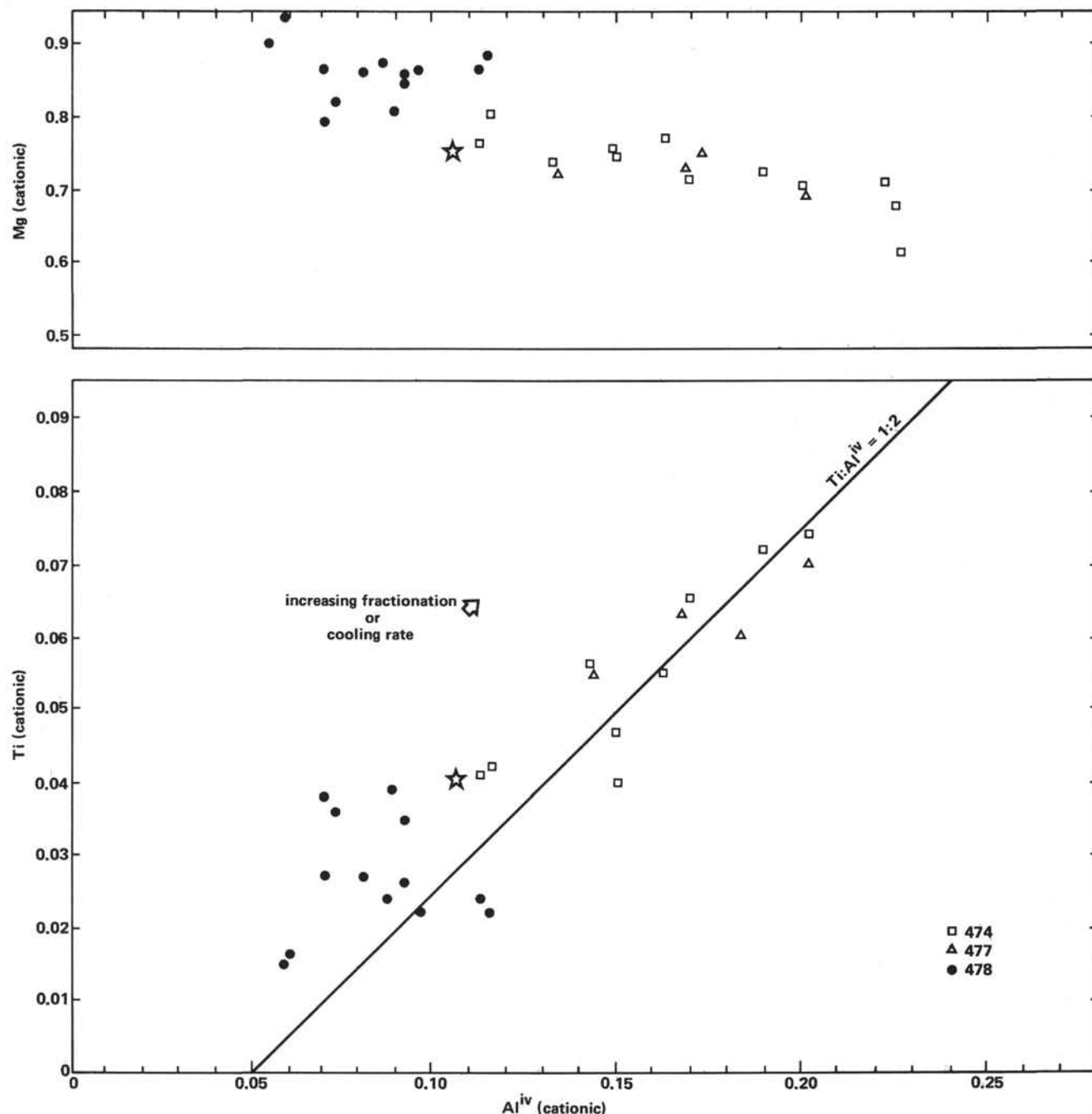


Figure 9. Plot of Mg and Ti versus calculated  $Al^{iv}$  in Leg 64 pyroxenes. ( $Ti-Al^{iv}$  [1:2] increases resulting from increased fractionation or increased cooling rate are diagrammatically shown. Stars represent the average composition of Leg 34 pyroxenes [Schweitzer et al., 1979].)

and predicted trace-element variations clearly indicate that in most cases simple closed-system crystal fractionation does not adequately explain all of the observed chemical and mineralogical features. In particular, it fails to explain (1) the common presence of An-rich plagioclase xenocrysts, (2) the inhomogeneous distribution of olivine and/or plagioclase in some units, (3) the presence of aluminous spinel in a few mafic samples, (4) the excessive enrichments of incompatible elements (e.g., Ti, Zr, P), and relatively small decreases in Ni and Cr in evolved basalts, and (5) the inverse relation between

$CaO/Al_2O_3$  and Mg number with little evidence of clinopyroxene fractionation.

Picritic basalts from Hole 474A (Mg numbers  $\sim 75$ ) could represent the composition of melts derived directly from the mantle (i.e., primary); however, they have noticeable excess concentrations of olivine phenocrysts ( $\pm$  spinel) and therefore may be cumulate. Spinel microphenocrysts in some olivine-rich basalts are an aluminous variety generally associated with picritic MORB. Fisk and Bence (1980) suggest that such spinels could crystallize in magmas enriched in MgO by the

Table 8. Least-squares fractionation calculations, Holes 474A, 475B.

Model Number	Parent Sample (level in cm)	Derivative Sample	Liq	Cpx	Plag <sub>An</sub>	Ol <sub>Fo</sub>	Spnl	$\Sigma r^2$	Comments
<b>474A</b>									
1	42-1, 6	40-2, 40	86.27			7.4990	7.67	0.673	
2	40-2, 40	39-3, 148	92.22			9.2790		0.887	+ FeO
3	40-2, 40	45-4, 64	80.84	3.04	3.9240	11.3 90		0.061	
4	46-3, 74	45-4, 64	84.42		10.4890	4.0990		0.677	- CaO
5	46-3, 74	45-4, 64	79.47	4.75	11.2590	3.6090		0.172	+ TiO <sub>2</sub> , + P <sub>2</sub> O <sub>5</sub>
6	46-3, 74	50-3, 91	71.93	6.42	17.0190	3.9785		0.193	+ P <sub>2</sub> O <sub>5</sub>
7	47-1, 127	50-4, 1	70.90	6.50	19.9974	3.4785		0.176	+ TiO <sub>2</sub> , + K <sub>2</sub> O
8	47-1, 127	50-3, 91	66.18	7.20	22.1075	4.8385		0.084	+ TiO <sub>2</sub>
9	47-1, 127	50-3, 91	51.01	11.47	29.9867	7.7090		0.039	
10	46-2, 112	49-1, 2	82.30	4.10	8.9390	4.2385		0.404	+ TiO <sub>2</sub> , - FeO
11	46-2, 112	49-2, 31	78.96	0.70	15.0978	5.2985		0.061	
12	46-2, 112	45-4, 64	87.63		7.8767	4.8285	1.25	0.085	+ TiO <sub>2</sub> , - K <sub>2</sub> O
13	42-1, 6	40-1, 19	92.99	0.25	4.3190	1.8890		0.160	+ TiO <sub>2</sub> , - Na <sub>2</sub> O
14	42-1, 6	40-1, 19	86.60	5.44	4.2940	1.5690	2.77	0.052	+ TiO <sub>2</sub>
15	40-1, 19	39-3, 148	66.53		10.3890	20.1790		0.974	- TiO <sub>2</sub> , - FeO, - K <sub>2</sub> O
16	42-1, 6	39-3, 148	68.73	4.06	5.4390	16.9690	6.08	0.108	- Na <sub>2</sub> O
17	48-1, 101	50-4, 1	81.70	6.30	10.6490	1.4890		0.310	+ TiO <sub>2</sub> , + P <sub>2</sub> O <sub>5</sub> , + K <sub>2</sub> O
<b>475B</b>									
18	4-1, 2	3-1, 2	85.88	2.49	5.3690	6.5286		0.048	
19	4-1, 2	3-1, 2	69.97	6.93	7.7190	14.1676		0.369	- Na <sub>2</sub> O, + P <sub>2</sub> O <sub>5</sub>
20	4-1, 2	2-1, 32	73.55	8.54	8.5473	8.0977		0.078	- Na <sub>2</sub> O
21	4-1, 2	2-1, 32	100.39		-5.7740	4.5590		0.920	+ TiO <sub>2</sub> , - CaO

Note: Subscripts for plagioclase (Plag) and olivine (Ol) refer to calculated best-fit compositions in terms of anorthite and forsterite components. A positive sign in the "Comments" column indicates that the oxide was calculated in excess in a parental liquid as compared to the measured value in the parent sample.

Table 9. Least-squares fractionation calculations, Guaymas Basin.

No.	Parent Sample (level in cm)	Derivative Sample	Liq	Cpx	Plag <sub>An</sub>	Ol <sub>Fo</sub>	Spnl	$\Sigma r^2$	Comments
<b>477-477A</b>									
1	12-4, 76	13-2, 146	90.96		0.5940	8.6383		0.051	
2	12-4, 76	13-2, 146	84.09	2.53	4.0140	9.1680		0.026	
3	12-4, 76	9-1, 57	72.30		15.3377	11.5479		0.026	
4	11-2, 61	13-2, 146	90.63		3.2290	6.6688		0.140	+ TiO <sub>2</sub> , - P <sub>2</sub> O <sub>5</sub>
5	11-2, 61	13-2, 146	64.87	7.14	17.7164	10.2375		0.018	- K <sub>2</sub> O, - P <sub>2</sub> O <sub>5</sub>
6	11-2, 61	9-1, 57	54.36	5.56	27.2473	12.3075		0.060	- K <sub>2</sub> O, - P <sub>2</sub> O <sub>5</sub>
7	12-4, 76	2-1, 7	85.95		6.3040	6.6472		0.171	- K <sub>2</sub> O, - P <sub>2</sub> O <sub>5</sub>
8	12-4, 76	2-1, 7	86.39	4.04	3.9246	4.8172		0.026	- K <sub>2</sub> O, - P <sub>2</sub> O <sub>5</sub>
9	12-4, 76	2-1, 7	100.00		-3.6990	2.7182		0.322	+ TiO <sub>2</sub> , + CaO, - K <sub>2</sub> O
10	12-4, 76	3-2, 17	73.57	5.99	7.8240	11.6976		0.071	- K <sub>2</sub> O, - TiO <sub>2</sub> , - P <sub>2</sub> O <sub>5</sub>
11	12-4, 76	3-2, 17	94.88	1.41	-5.4886	8.6384		0.006	
<b>478</b>									
12	42-2, 80	43-2, 104	49.88	6.50	29.6156	10.2571		0.096	+ TiO <sub>2</sub> , - K <sub>2</sub> O, - P <sub>2</sub> O <sub>5</sub>
13	42-2, 80	51-3, 49	32.47	9.08	36.9162	17.5371		0.135	- Na <sub>2</sub> O
14	49-1, 63	51-3, 49	33.38	9.41	36.9271	17.2272		0.148	- Na <sub>2</sub> O, + K <sub>2</sub> O
15	49-1, 63	51-3, 49	18.31	14.14	46.4865	16.3771	2.04	0.008	- P <sub>2</sub> O <sub>5</sub>
16	49-1, 63	43-2, 104	53.60	6.17	28.1268	9.3671		0.015	- K <sub>2</sub> O, - P <sub>2</sub> O <sub>5</sub>
17	49-1, 63	43-2, 104	78.76		14.5782	4.6786		0.160	+ TiO <sub>2</sub> , - K <sub>2</sub> O
18	54-1, 77	54-4, 2	63.54	4.59	24.0064	7.6076		0.088	- K <sub>2</sub> O
19	49-1, 63	13-2, 146	52.95	7.64	25.4962	11.1975		0.012	- K <sub>2</sub> O, - P <sub>2</sub> O <sub>5</sub>
20	49-1, 63	13-2, 146	85.43		6.3370	6.5490		0.015	+ TiO <sub>2</sub> , + P <sub>2</sub> O <sub>5</sub>
<b>481A</b>									
21	16-2, 111	15-3, 27	76.77	8.27	11.3760	2.4890	0.44	0.081	+ K <sub>2</sub> O
22	16-2, 111	15-3, 115	79.49	8.01	9.0477	3.1090		0.023	+ K <sub>2</sub> O
23	17-2, 6	15-3, 27	83.58	6.00	6.0090	4.2986		0.130	+ K <sub>2</sub> O, + P <sub>2</sub> O <sub>5</sub>
24	17-2, 6	33-1, 91	83.48	0.30	9.6769	6.3190		0.088	+ K <sub>2</sub> O
<b>478-481A</b>									
25	49-1, 63	15-3, 27	38.32	10.00	35.7472	12.9371		0.050	
26	49-1, 63	17-2, 6	42.56	8.36	34.4472	11.7571		0.087	- Na <sub>2</sub> O, - K <sub>2</sub> O

Note: As in Table 8.

addition of forsteritic olivine. This implies that even though olivine may have accumulated by post-emplacement gravitational settling, spinel could have formed *in situ* and not have been a fractionating phase. The fact that none of the natural glasses recovered during Leg 64 (Fornari et al., this volume) has compositions as mafic as the picritic basalts is further evidence that such "primary" liquids were not erupted. None of the natural glasses recovered during Leg 64, however, was from a unit with chemistry similar to Units 1 and 2a from Hole 474A. Consequently, while the chemistry of these units may in part result from cumulus olivine, it is possible that other mechanisms were involved in giving these rocks their unusual depleted trace-element chemistry.

The most primitive, noncumulate basalts from Leg 64 have Mg numbers ~ 60 to 70 and compositions similar to basalts from other ocean-ridge environments that are considered "primitive" MORB (see Dungan and Rhodes, 1978; Bender et al., 1978; Clague and Bunch, 1976). The lack of primary picritic basalts and extreme differentiates may be a consequence of their greater density compared to "primitive" MORB (Sparks et al., 1980; Stolper and Walker, 1980) or result from an efficient magma mixing, which results in an abundance of moderately evolved basalts (Dungan and Rhodes, 1978; Walker et al., 1979). The latter mechanism has great applicability, because it can explain the presence of xenocrysts, the anomalous enrichment of incompatible ele-

ments, and the major-element variations resulting from cryptic clinopyroxene fractionation.

The presence of An-rich plagioclase xenocrysts that are clearly not in equilibrium with their host basalts suggests that the xenocrysts originally crystallized in more primitive magmas having higher Ca/Ca + Na and Mg/Mg + Fe ratios. Similar arguments, based on Fe/Mg equilibration, hold for the forsteritic olivines found in some of the olivine-rich basalts. These features have been used as evidence for the mixing of primitive magmas and their phenocrysts into fractionating magma bodies containing more evolved basalts (Rhodes et al., 1979; Shibata et al., 1979).

One consequence of such magma mixing might be the development of inhomogeneous distributions of phenocrysts within single igneous units, as has occurred in Holes 474 and 477. If the injection of primitive magma occurred at depths greater than ~20 km (~6 Kbar), then plagioclase (An<sub>90</sub>) would have had a tendency to float in basaltic magmas because of the increased melt density with pressure (see Flower, 1980), whereas olivine would have sunk, eventually producing evolved basalts, rich in plagioclase, and basal picritic basalts such as those sampled in Holes 474 and 477.

Most of the glassy and slightly phyric basalts drilled during Leg 64 contain phenocrysts of plagioclase or olivine, which suggests that they are liquidus phases. This observation conforms to the liquidus phase relations in "primitive" MORB at low pressure (1 atm.; Bender et al., 1978; Walker et al., 1979). Experimental work has also shown that clinopyroxene does not coexist with Ol + Plag until ~75–100°C below the liquidus, by which time liquids are nearly 50% crystallized (Bender et al., 1978; Walker et al., 1979).

Many of the fractionation models we present indicate that significant amounts of clinopyroxene must be extracted with Ol + Plag to adequately explain the observed major-element variations; but this is not compatible with the observed or experimental phase relations. This enigma is encountered in fractionation models derived for other MORB suites (e.g., Clague and Bunch, 1976; Shibata et al., 1979; Byerly, 1980).

The presence of clinopyroxene phenocrysts in relatively few basalts and in a number of gabbros from Leg 64 provides some evidence that crystallization may have been initiated above ~10 Kbar, where clinopyroxene is a liquidus phase.

This may explain the origin of cumulate clinopyroxene layers and clinopyroxene-rich gabbros, but the fractionating magmas would have to move to higher levels (<10 kb) and continue fractionating Ol + Plag to produce the observed chemical changes. Such a polybaric fractionation scheme, as proposed by Flower (1980), also has the potential to explain the formation of plagioclase-rich differentiates by crystal flotation and accumulation. The lack of clinopyroxene xenocrysts in the Leg 64 basalts does not support this scheme; however, the rather restricted nature of our sampling technique does not completely preclude it.

Magma mixing/fractionation models recently discussed by Dungan and Rhodes (1978), Rhodes et al.

(1979), and Walker et al. (1979) appear to most adequately explain the chemical variations observed in basalts from Leg 64. In particular, mixing primitive and differentiated basalts can produce liquids in which Cpx (+ Plag) will crystallize before Ol (Walker et al., 1979). This mechanism relies heavily on the development of reasonably evolved basalts (that crystallize Cpx before Ol) by simple crystal fractionation prior to mixing; but if mixing is efficient, no end-members will remain. Linear mixtures of these end-members will produce a liquid composition reflecting the fractionation that previously occurred in the primitive and differentiated melts (Walker et al., 1979). Consequently, least-squares calculations suggesting extensive three-phase fractionation may simply be a consequence of Ol + Plag and Cpx + Plag crystallization prior to the mixing of two evolving liquids. Furthermore, Walker et al. (1979) suggest that subophitic textures—such as those in many of the Leg 64 basalts—may, as a result of mixing, be a consequence of supercooling below the three-phase saturation temperature.

Another important consequence of magma mixing observed in some basalts from Leg 64 is the anomalous enrichment of incompatible elements with little change in compatible element contents. The result of mixing a primitive magma even with small amounts of a highly differentiated liquid is a hybrid magma with incompatible element contents in excess of that predicted by Rayleigh fractionation while continuously buffering compatible elements such as Cr and Ni (Dungan and Rhodes, 1978; Rhodes et al., 1979).

To date, the effects of magma mixing and fractional crystallization have been evident only in basalts generated at slow spreading ridges in the Atlantic. The physical and tectonic processes that control such mechanisms exist in areas—such as the Gulf of California—that experience more rapid spreading rates.

#### REFERENCES

- Bence, A. E., Baylis, D. M., Bender, J. F., et al., 1979. Controls on the major and minor element chemistry of mid-ocean ridge basalts and glasses. In Talwani, M., Harrison, C. G., and Hayes, D. E. (Eds.), *Deep Drilling Results in the Atlantic Ocean: Ocean Crust*: Washington (American Geophysical Union), pp. 331–341.
- Bender, J. F., Hodges, F. N., and Bence, A. E., 1978. Petrogenesis of basalts from the Project FAMOUS area: Experimental study from 0–15 kb. *Earth Planet. Sci. Lett.*, 41:277–302.
- Byerly, G., 1980. The nature of differentiation trends in some volcanic rocks from the Galapagos spreading center. *J. Geophys. Res.*, 85:3797–3810.
- Clague, D. A., and Bunch, T. E., 1976. Formation of ferrobasalts at east Pacific midocean spreading centers. *J. Geophys. Res.*, 81: 4247–4256.
- Coish, R. A., and Taylor, L. A., 1979. The effects of cooling rate on texture and pyroxene chemistry in DSDP Leg 34 basalts: A microprobe study. *Earth Planet. Sci. Lett.*, 42:389–398.
- Dungan, M. A., and Rhodes, J. M., 1978. Residual glasses and melt inclusions in basalts from DSDP Legs 45 and 46: Evidence for magma mixing. *Contrib. Mineral. Petrol.*, 67:417–431.
- Fisk, M. R., and Bence, A. E., 1980. Experimental crystallization of chrome spinel in FAMOUS basalt 527-1-1. *Earth Planet. Sci. Lett.*, 48:111–123.
- Flower, M. F. J., 1980. Accumulation of calcic plagioclase in ocean-ridge tholeiite: An indication of spreading rate? *Nature*, 287: 530–532.

- Mazzullo, L. J., and Bence, A. E., 1976. Abyssal tholeiites from DSDP Leg 34: The Nazca Plate. *J. Geophys. Res.*, 81:4237-4351.
- Papike, J. J., Cameron, K. L., and Baldwin, K., 1974. Amphiboles and pyroxenes: Characterization of other than quadrilateral components and estimates of ferric iron from microprobe data. *Geol. Soc. Am. Abstract with Programs*, 6:1053-1054. (Abstract)
- Perfit, M. R., Fornari, D. J., Malahoff, A., et al., 1980. Geochemistry and mineralogy of MORB, FETI basalts and andesites from the Galapagos Rift. *Trans. Amer. Geophys. Union (EOS)*, 61: 1143.
- Rhodes, J. M., Dungan, M. A., Blanchard, D. P., et al., 1979. Magma mixing at mid-ocean ridges: Evidence from basalts drilled near 22°N on the Mid-Atlantic Ridge. *Tectonophysics*, 55:35-61.
- Schweitzer, E. L., Papike, J. J., and Bence, A. E., 1979. Statistical analysis of clinopyroxenes from deep-sea basalts. *Am. Mineral.*, 64:501-513.
- Shibata, T., DeLong, S. E., and Walker, D., 1979. Abyssal tholeiites from Oceanographer Fracture Zone I. Petrology and fractionation. *Contrib. Mineral. Petrol.*, 70:89-102.
- Sigurdsson, H., and Schilling, J.-G., 1976. Spinel in Mid-Atlantic Ridge basalts: Chemistry and occurrence. *Earth Planet. Sci. Lett.*, 29:7-20.
- Sparks, R. S. J., Meyer, P., and Sigurdsson, H., 1980. Density variation amongst mid-ocean ridge basalts: Implications for magma mixing and the scarcity of primitive lavas. *Earth Planet. Sci. Lett.*, 46:419-430.
- Statham, P. J., 1976. A comparative study of techniques for quantitative analysis of the X-ray spectra obtained with a Si(Li) detector. *X-Ray Spectrom.*, 5:16-28.
- Stopler, E., and Walker, D., 1980. Melt density and the average composition of basalt. *Contrib. Mineral. Petrol.*, 74:7-12.
- Sweatman, T. R., and Long, J. V. P., 1969. Quantitative electron-probe microanalysis of rock-forming minerals. *J. Petrol.*, 10: 332-379.
- Walker, D., Kirkpatrick, R. J., Longhi, J., et al., 1976. Crystallization history of lunar picritic basalt sample 12002: Phase-equilibria and cooling rate studies. *Geol. Soc. Am. Bull.*, 87:646-656.
- Walker, D., Shibata, T., and DeLong, S. E., 1979. Abyssal tholeiites from the Oceanographer Fracture Zone, II. Phase equilibria and mixing. *Contrib. Mineral. Petrol.*, 70:111-125.
- Wilkinson, J. F. G., in press. The genesis of mid-ocean ridge basalt. *Earth Sci. Rev.*